Journal of The
Electrochemical Society

Mechanisms of Secondary Spreading and Micro Droplet Formation on Steel

To cite this article: Lea Seeger *et al* 2024 *J. Electrochem. Soc.* **171** 121504

Journal of The Electrochemical Society, 2024 **171** 121504

Mechanisms of Secondary Spreading and Micro Droplet Formation on Steel

Lea Seeger,[1,z] Renate Lobnig,[1] Elmar Schuch,[2] Surong Guo,[1] and Wolfram Fürbeth[3]

[1]*University of Applied Science, Esslingen, Faculty of Science, Energy and Building Services, Esslingen, BW 73728, Germany*
[2]*University of Applied Science, Esslingen, Faculty of Mechanical and Systems Engineering, Esslingen, BW 73728, Germany*
[3]*Dechema-Korrosionszentrum, Frankfurt am Main, Frankfurt am Main 60486, Germany*

A new theory for secondary spreading based on the wetting theory of thin films is presented. It explains how micro droplets within the spreading zone and the primary droplet retain their shape, although connected by a thin electrolyte film and how humidity and salt concentration affect the growth rate of micro droplets. The trigger for secondary spreading, polarization or alkalization, is identified by using droplets of sodium hydroxide solution. Secondary spreading thus occurs on steel from pH 13.5 without corrosion or external polarization. The limiting pH value found explains why secondary spreading on steel only occurs when certain salts are used. The effect of the substrate is investigated by changing the microstructure of the steel. By comparing the sizes of micro droplets and micro structural phases and by scanning electron microscopy/energy-dispersive X-ray analysis measurements of the spreading zone, the existence of an electrolyte film connecting the micro droplets is supported. E_{corr} potential profiles of secondary spreading droplets of sodium chloride solution on steel acquired by means of SKP are used to assess the contribution of secondary spreading to the total corrosion current, which is estimated to be low compared to that of the cathodic zone at the edge of the droplet.

 [DOI: 10.1149/1945-7111/ad9bf3]

Manuscript submitted October 15, 2024; revised manuscript received December 5, 2024. Published December 23, 2024.

Secondary spreading of an electrolyte droplet on metal is a corrosion phenomenon, in which a thin electrolyte film or micro droplets spread outward from a primary droplet, while the shape of the primary droplet is retained. The spreading rate follows a $\sqrt{t}$-function.[1–3] During secondary spreading, the anode with the lowest potential is located in the center under the primary droplet. The cathode, on the contrary is located at the edge of the droplet and in the spreading zone. The cathode is at a higher potential and the spreading zone widens the cathode beyond the edge of the droplet. Around the spreading zone is the periphery, the unwetted metal surface, at the highest potential.[1–4] Metal dissolution mainly takes place at the anode and oxygen reduction at the cathode with the formation of OH^- ions. This is why the pH value at the droplet edge and in the spreading zone rises sharply.[1–5]

Secondary spreading is not yet fully understood and there are some open questions:

- What triggers secondary spreading and what is the mechanism for secondary spreading?
- Under which conditions do micro droplets or a thin electrolyte film form? Can micro droplets and electrolyte film coexist? If the micro droplets form on a thin electrolyte film, how do the micro droplets and also the primary droplet remain their shape and why don't they merge into a large flat droplet?
- What defines the growth rate of the spreading zone and the micro droplets and why does secondary spreading occur with some combinations of substrate and salt solution and not with others?
- What proportion of the metal loss is due to secondary spreading compared to corrosion within the droplet?

In the following the results of other studies will be discussed, before the questions will be addressed with our own experimental results.*What triggers secondary spreading and what is the mechanism for secondary spreading?*

Secondary spreading has so far only been observed in combination with corrosion on zinc, copper, iron and steel or with external cathodic polarization additionally on stainless steel and platinum.[1–3,5–7] In an oxygen-free atmosphere without external polarization, secondary spreading does not occur due to the lack of oxygen reduction.[1,6] Similarly, secondary spreading also does not occur on inert substrates like stainless steel and platinum without external polarization.[3,6] However, secondary spreading can also be simulated with inert substrates or in an oxygen-free atmosphere by cathodic polarization of the substrate.[3,6,7] In the studies of Zhang et al. and Wang et al., it is pointed out that it is not the oxygen reduction itself, but the polarization or the flowing corrosion current that could be decisive for the secondary spreading.[6,7] However, neither J. Zhang et al. nor J. Wang et al. used a reference electrode, so that only the potential difference between anode and cathode is known, but not the potential of the cathodically polarized substrate. It cannot be ruled out that cathodic water decomposition occurred during polarization, which can lead to an increase in the pH value. This means that, as with corrosion, the spreading could have been caused by the rising pH value and not primarily by polarization. The question remains: Does cathodic polarization or alkalization of the cathodic zone due to oxygen reduction cause secondary spreading?

A wide spread theory for secondary spreading is that alkalization at the droplet edge caused by oxygen reduction or cathodic polarization strongly changes the energy of the metal oxide surface/electrolyte interface, which leads to destabilization of the droplet shape and spreading.[1,8] However, this theory does not explain the stability of the primary droplet surrounded by a liquid film. Reducing the contact angle should lead to flattening the primary droplet while increasing the contact area with the substrate. However, in reality the original droplet shape is maintained while an electrolyte layer spreads around the droplet. Another aspect that Tsuru et al. address and which is still open, is the question of how the micro droplets retain their shape.[3] If one assumes that micro droplets form on a thin electrolyte layer, they should also deliquesce on the film.

Schindelholz et al. put forward an alternative theory for copper. Alkalization at the droplet edge leads to the dissolution of the oxide film on copper and the exposure of the bare metal surface. Its high surface energy leads to spreading of the droplet.[9] However, Schindelholz's theory only explains secondary spreading on metals whose oxides are soluble in the strongly alkaline range. Iron, for example, forms a dense passive layer in alkaline medium. Also, the theory does not explain how the primary droplet retains its shape when surrounded by a liquid film.

Wang et al. assumes that micro droplets form due to cathodic polarization, which decreases the local surface tension of the liquid/

[z]E-mail: lea.seeger@hs-esslingen.de

metal interface and cools the metal surface near the three-phase boundary by a Peltier effect. This leads to local liquid evaporation and condensation on the nearby metal surface.[7] However, this theory does not explain the salts found in the micro droplets. To balance the charge, anions migrate to the anode in the center of the droplet and cations migrate to the cathodic spreading zone. In the spreading zone, CO_2 from the atmosphere can be absorbed by the high pH value, so that carbonates (with NaCl electrolyte sodium carbonate) are often found there.[1,4,8,10,11] In addition, the pH of condensed water would be neutral and not strongly alkaline. Moreover, the observation of a thin electrolyte film is not covered by this theory.

To the best of our knowledge, no theory has yet been presented that fully describes all observations.*Under which conditions do micro droplets or a thin electrolyte film form? Can micro droplets and electrolyte film coexist? If the micro droplets form on a thin electrolyte film, how do the micro droplets and also the primary droplet remain their shape and why don't they run on it to form a large flat droplet?*

In some cases, instead of a thin electrolyte film or additionally to that film, the formation of micro droplets around the primary droplet has been reported.[3,4,8,11] To the best of our knowledge, it is not clear from the literature under which conditions an electrolyte film or micro droplets form. It seems that these two forms are manifestations of the same phenomenon. Electrolyte film and micro droplets could coexist and micro droplets could therefore form in addition to the spreading of the electrolyte film. For example, Neufeld et al. reported a wetting front forming from a droplet of NaCl solution on zinc, recognizable by a change in color, which precedes the formation of micro droplets. He explained this with a thin electrolyte film that connects the micro droplets.[12] Schindelholz et al. described something comparable on copper.[9] On iron, on the other hand, Neufeld et al. could see micro droplets but no thin electrolyte film. He suspected that a possible electrolyte film could be too thin for detection. If a thin electrolyte film connects the micro droplets, the question remains how the micro droplets and also the primary droplet are stable on this electrolyte film and why they do not merge. *What defines the growth rate of the spreading zone and the micro droplets and why does secondary spreading occur with some combinations of substrate and salt solution and not with others?*

Risteen et al. raised the question, what determines the area of the spreading zone. It was assumed that there could be substrate-specific effects, because the observed spreading zone of droplets of NaCl solution was significantly larger on steel than on pure iron.[13]

Factors that lower the pH value of the electrolyte can slow down secondary spreading. Thus, a generally slower spreading was observed in atmospheres containing CO_2 and especially in atmospheres containing SO_2. This can also be caused by acidification of the electrolyte with sulphuric acid.[1,2,8,10,11] Also dissolved salts can influence secondary spreading. Why secondary spreading does not occur with some combinations of substrate and salt solution is not yet fully understood. First systematic experiments with different salts were undertaken by Zhang et al. and Tsuru et al.[3,6] In general, high humidity and a high salt concentration have an accelerating effect on secondary spreading.[3,14] Zhang et al. and also Tsuru et al. describe that the spreading zone of a NaCl droplet on steel is larger in higher humidity. Tsuru et al. concludes, that there could be water uptake by absorption from air.[3,6]*What proportion of the metal loss is due to secondary spreading compared to corrosion within the droplet?*

This question was raised by Schindelholz et al.[9] If the spreading zone is part of the cathodic zone, then secondary spreading causes a significant increase in the cathodic zone of a corroding droplet beyond the edge of the droplet and could potentially greatly increase the corrosion current.

The aim of this paper is to clarify the described questions.

Experimental

Materials.—The substrate used is thin sheet steel DC 01 with material number 1.0330 (according to EN 10027–1 and EN 10027–2) with a thickness of 0.88 mm. The chemical composition of the steel is according to EN 10130: 2006 C_{max} 0.12%, P_{max} 0.045% and S_{max} 0.045%.[15] Pure iron "Alliedpureiron" from PURON Metals with 0.002% C (purity >99.8%) and 1.5 mm thickness is used for comparison. The electrolytes used are 1% NaCl solution, NaOH solutions of various concentrations up to 8 molar and 1 molar KOH and LiOH solutions. NaCl and LiOH are purchased from Carl Roth GmbH + Co KG with a purity of ⩾99% and KOH as a titer solution with a concentration of 1 mol l^{-1} +/−0.2%. The pH value of the NaOH solutions is measured using a pH electrode (Lab 860 with Schott pH Electrode Blue Line 14 pH, 3 M KCl, with integrated thermometer, Schott Instruments), which was previously calibrated with three buffer solutions (Roticalpure, pH 4.7.10 +/−0.02 at 20 °C, Carl Roth GmbH + Co. KG). The pH value is also checked with pH sticks (pH-Fix, pH 0–14, Carl Roth GmbH).

Sample preparation.—Sample sheets measuring $3 \times 3\ cm^2$ are cleaned for 5 min in an ultrasonic bath with acetone, then ground in stages to 600 grit and polished to a mirror finish with 1 μm diamond paste. Immediately after polishing, the samples are rinsed with deionized water, acetone and again with deionized water and dried with tissue paper. This is immediately followed by storage in a self-built humidity chamber over saturated magnesium nitrate solution at 57% RH and 25 °C for 24 h. Experiments are carried out immediately after storage.

SKP measurement of corroding NaCl droplets on steel.—The Scanning Kelvin Probe used is from Wicinski-Wicinski GbR with automatic height control and temperature and humidity control. The probe with 178 μm diameter is made of nickel. The measuring distance of the Volta potential difference $\Delta\Psi$ is 40 μm. This distance proved to be suitable in previous measurements. Smaller ones led to difficulties in height control. The vibrating amplitude of the nickel probe is 5 μm. All experiments with the Kelvin Probe are performed at 25 °C and 95% relative humidity. Before each measurement, the Kelvin Probe is calibrated for one hour over a Cu/saturated $CuSO_4$-halfcell to convert the measured voltaic potential difference $\Delta\Psi$ into E_{corr} values. E_{corr} of the Cu/saturated $CuSO_4$-halfcell was determinated by measuring directly against a Ag/AgCl/3 molar KCl reference electrode at room temperature, for 2 h. The potential of the Cu/sat. $CuSO_4$-halfcell with 0,311 +/−0,002 V is only slightly below the literature value of 0,317 V vs SHE.[16]

The relationship between $\Delta\Psi$ and E_{corr} is:[17,18]

$$E_{corr} = \frac{\Phi^{KP}}{e} - E_{ref} + \Delta\Psi = const. + \Delta\Psi \qquad [1]$$

- Φ^{KP} = work function of the Kelvin Probe
- e = charge of an electron
- Ψ^{KP}—Ψ^{S} = $\Delta\Psi$ = Volta potential difference between Kelvin Probe and sample
- E_{corr} = electrode potential difference between a sample and a reference electrode
- E_{ref} = absolute electrode potential of the reference electrode (in most studies the absolute electrode potential of the SHE is to be used as E_{ref}. According to the IUPAC recommendation, this is 4.44 +/− 0.02 V at 298.15 K [19])

In an earlier publication[20] it was shown that the work function of the nickel probe used and thus the constant const. changes with the relative humidity and that it is not the humidity in the environment but the humidity at the tip of the probe that is decisive. It was also demonstrated that if measurements are taken at a very small distance of 40 μm above the surface of an aqueous electrolyte at 25 °C, the relative humidity at the probe tip corresponds approximately to the humidity directly above the electrolyte surface. For calibration

above the Cu/saturated $CuSO_4$-halfcell, the humidity above the saturated solution and at the tip of the probe is approximately equal to the critical relative humidity. This is 98% RH for $CuSO_4$.[21] The constant const. determined during the calibration therefore applies to a RH of 98%.

For the SKP measurement on steel, it is assumed that the relative humidity at the probe tip is not changed by materials with negligibly low water vapor partial pressure, like the used steel substrate, and thus corresponds to the ambient humidity of 95% RH. When measuring in a sufficiently small distance above droplets, the local humidity at the tip of the probe approximates the humidity directly above the solution surface. This humidity can be estimated by the salt concentration in the droplet. Initially a single droplet of 1 w% NaCl solution is placed on polished steel. Assuming an ideal solution, Raoult's law can be used to calculate the reduction of the water vapor pressure due to the dissolved salts:[22]

$$p_{H_2O} = x_{H_2O} p^{\circ}_{H_2O} \qquad [2]$$

- p_{H2O} = Partial water vapor pressure/unit Pa
- x_{H2O} = Molar fraction of water/unit -
- p°_{H2O} = Vapor pressure of the pure liquid water/unit Pa

The vapor pressure of the solid component is neglected, as is the influence of the curvature of the droplets on the vapor pressure. The density of the salt solution is assumed to be 1 kg l^{-1}. This means that for a 1% NaCl solution (0.171 mol l^{-1}), the molar fraction of water x_{H2O} is given by:

$$x_{H_2O} = \frac{n_{H_2O}}{n_{H_2O} + n_{Na^+} + n_{Cl^-}} = \frac{54,95\text{mol}}{54,95\text{mol} + 2 \cdot 0,171\text{mol}} = 0,994 \qquad [3]$$

This means that the water vapor partial pressure of the salt solutions is 0.6% lower than that of pure water and the relative humidity directly above the salt solution is 99.4%. As the droplets dry out, the salt concentration increases. As a result, the water vapor partial pressure or relative humidity above the solution also decreases until the water vapor partial pressure or relative humidity above the solution corresponds to that of the environment. The humidity above a drying droplet thus drops to a minimum of 95% RH at an ambient humidity of 95% RH. This also applies if other or additional ions are formed from the original ions due to corrosion reactions.

At an ambient humidity of 95% RH, the probe tip of the SKP is exposed to a humidity of 99.4% RH to 95% RH according to these considerations. Calibration takes place at 98% RH. According to[20] this small deviation in relative humidity does not result in a significant change in the constant const. in Eq. 1.

Modification of the steel structure by annealing.—Different annealing processes of the steel used with a carbon content of 0.12% are employed to produce samples that do not differ in the composition of the steel, but do differ in the microstructure and the distribution of the carbon phase in the microstructure. It is assumed that the secondary spreading (spreading speed of the spreading zone and growth rate of micro droplets) is influenced by the inhomogeneity of the substrate surface.

The different annealing variants, soft annealing, normal grain annealing and large grain annealing are intended to change different aspects of the microstructure.

Soft annealing.—With this annealing variant, only the carbon precipitates in the steel are to be increased or reduced while retaining the original microstructure. The samples are annealed for 3.5 h at a constant temperature of 700 °C. This temperature is below the transformation temperature of α-Fe (ferrite) to γ-Fe, so that the original ferrite grains that make up the microstructure are retained. At 700 °C, however, the solubility of carbon in the ferrite is higher than at room temperature, so that carbon from precipitates can dissolve in the ferrite during the annealing time of 3.5 or 5 h. During cooling, the solubility of carbon in the ferrite decreases again and carbon can precipitate again. As this takes time, it is assumed that more or less carbon is precipitated depending on the cooling rate. In order to obtain samples with different amounts of precipitated carbon, the samples were cooled after annealing either very quickly by immersion in cold water, slowly by cooling in the switched-off furnace with the furnace door open or very slowly in the switched-off furnace with the furnace door closed (temperature curves see Fig. 1).

Normal grain annealing and large grain annealing.—In these annealing variants, the steel is heated above the transformation temperature from α-Fe (ferrite) to γ-Fe so that the original microstructure is dissolved. This forms γ-Fe grains, which grow with the annealing time and temperature. During normalizing, the steel sheets are annealed for 2 h at 900 °C, whereby smaller grains are formed than during large-grain annealing for 5 h at 1100 °C.

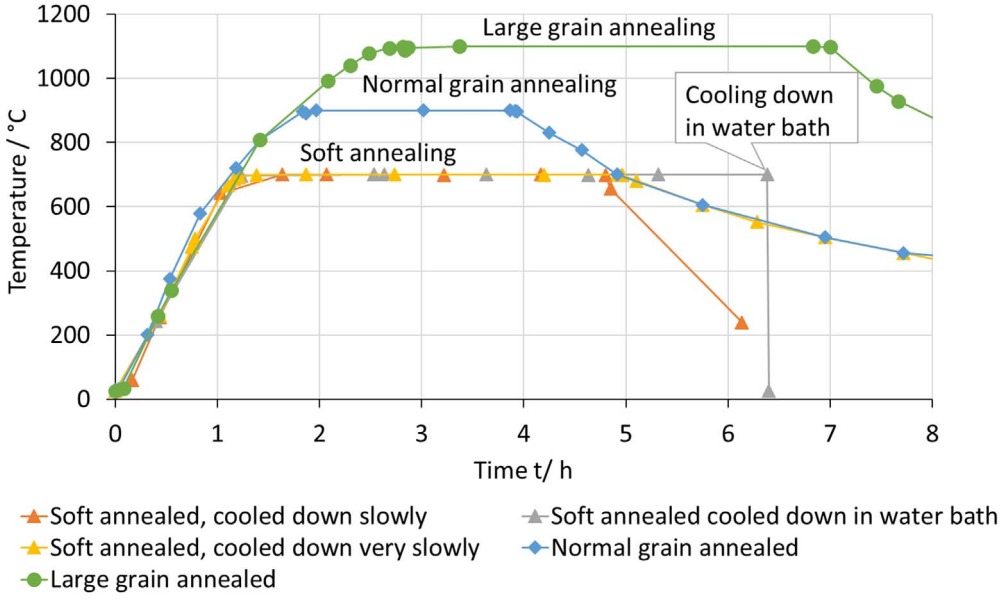

Figure 1. Temperature during annealing and cooling of the samples with different annealing variants.

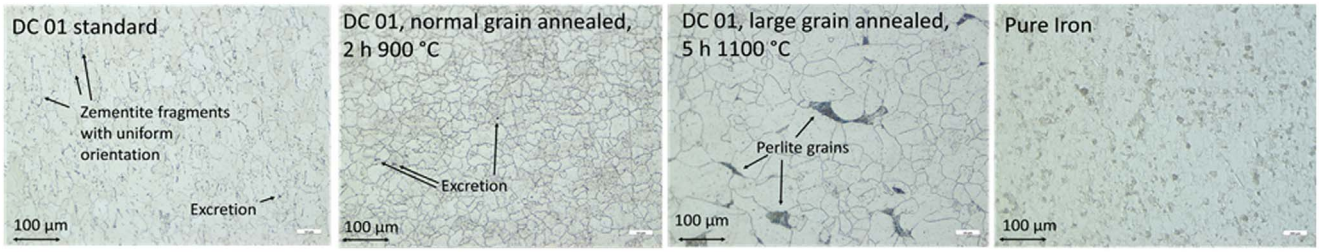

Figure 2. Optical microscopy images of the microstructure of the steels used and the pure iron after visualization by nital etching.

After annealing, the samples are cooled as slowly as possible for several hours in both variants so that the γ-Fe transforms back into α-Fe. The formation of phases far from equilibrium is avoided by the slow cooling of the samples after annealing. With rapid cooling, phases far from equilibrium such as bainite and martensite could form.

For all types of annealing a muffle furnace model M 110 thermicon P from Heraeus Instruments is used. The temperature during annealing and cooling is shown for all variants in Fig. 1. Oxidation during the annealing process is prevented by wrapping the steel sheets in stainless steel foil.

The steel microstructure is visualized by nital etching with freshly prepared 3% nital solution (0.6 ml concentrated HNO_3 solution to 20 ml ethanol) and the grain size is measured by the circular section method in 3-fold determination.[23] The Axio Imager. M2 optical microscope with EC Epiplan 10x/0.25 HD M27 objective is used for this purpose.

The grain sizes of the steels and the pure iron used are shown in Table I and the microscopic images of the microstructures are shown in Fig. 2.

The standard steel has a ferritic microstructure, with the ferrite grains containing fragments of cementite arranged in a linear pattern. The latter were probably formed by rolling and normalizing in the steelworks.

As expected, soft annealing at 700 °C with rapid cooling leaves a higher amount of carbon dissolved in the ferrite grains, while slow cooling causes the excess carbon to accumulate in precipitates. An accumulation of carbon within the precipitates was found with SEM/EDX in the samples cooled very slowly over several hours. However, as the soft annealing of the steel shows no significant influence on the growth rates of the spreading zone and the micro droplets in the following experimnets, a detailed description of the SEM/EDX measurements is not provided. Etching and microscopy of the microstructure of the soft-annealed steels revealed no significant deviation from the microstructure of the untreated standard steel. It is therefore not shown in Fig. 2.

Normalizing increases the average grain size only slightly, but leads to a significantly more uniform grain size distribution. Cementite fragments are completely dissolved and carbon is preferentially deposited at grain boundaries in round precipitates.

Large grain annealing significantly increases the average grain size, the size distribution becomes somewhat broader and carbon precipitates mainly appear as large lamellar pearlite grains.

Pure iron has a slightly larger average grain size than normalized steel. Precipitates are only rarely and sporadically found.

Measurement of the growth rates of the spreading zone and micro droplets.—The secondary spreading of 100 µl droplets of NaCl, NaOH, KOH and LiOH solution is tracked by optical microscopy at room temperature using Axio Imager.M2 with objective EC Epiplan 5x/0.13 HD M27. The humidity is maintained at 95% RH by a self-built sample chamber, in which the bottom is covered with saturated Na_2SO_4 solution (critical RH of Na_2SO_4: 95% RH at 25 °C[24]). After loading the chamber with a steel plate and a waiting time of 2 h, the droplet is applied through a suitable hole in the lid using a microliter syringe. The humidity inside the chamber is adjusted to the RH within the 2 h waiting time, which was tested by coalescence of Na_2SO_4 crystals. Due to the high magnification of the microscope, only a small area of the droplet edge can be observed. This area is observed for 2 h and images are taken at regular intervals, from which the movement of the contact line, the width of the spreading zone W_{SP} and the greatest length of the three largest micro droplets L_M are subsequently measured out using the IrfanView software. Examples for measuring the parameters are shown in Fig. 3.

From the 2 h observation of one droplet section, the growth laws and the growth rate of the spreading zone m_{SP} and the micro droplets m_M are determined. Using the growth laws from the 2 h observation, the growth rate of the spreading zone m_{SP} and the micro droplets m_M can also be determined from images of four further sections of the droplet edge taken after 2 h. The growth rate is calculated by converting Eq. 6 or Eq. 7 to m_{SP} or m_M. This provides averaged values for the entire droplet. A period of 110 min was assumed for the growth of the spreading zone, as the droplets are pinned after 10 min on average and the spreading zone can then grow largely undisturbed.

SEM/EDX measurements.—The JSM-7200F scanning electron microscope from JEOL is used for imaging SEM in secondary electron modus. The elemental analysis is carried out with a SEM-based energy-

Table I. Grain sizes of the steels and the pure iron used, determined using the circular section method. The mean values with simple standard deviation from 3 measurements are given. In the case of pure iron, 5 measurements were carried out due to the less uniform grain size.

		Grain size/µm	
Substrate	Annealing	Mean value	Single standard deviation
Standard steel (DC01)	—	21,9	2,7
Normal grain annealed (DC01)	2 h, 900 °C	22,6	0,5
Large grain annealed (DC01)	5 h, 1100 °C	32,3	5
Pure iron	—	24,2	2,7

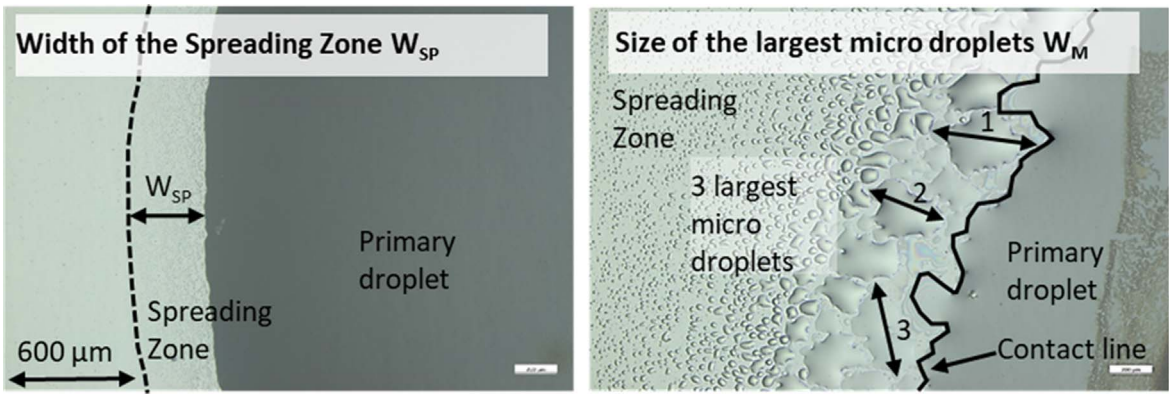

Figure 3. One example each for reading out the width of the spreading zone W_{SP} and the average size of the three largest micro droplets L_M from the optical microscopy images.

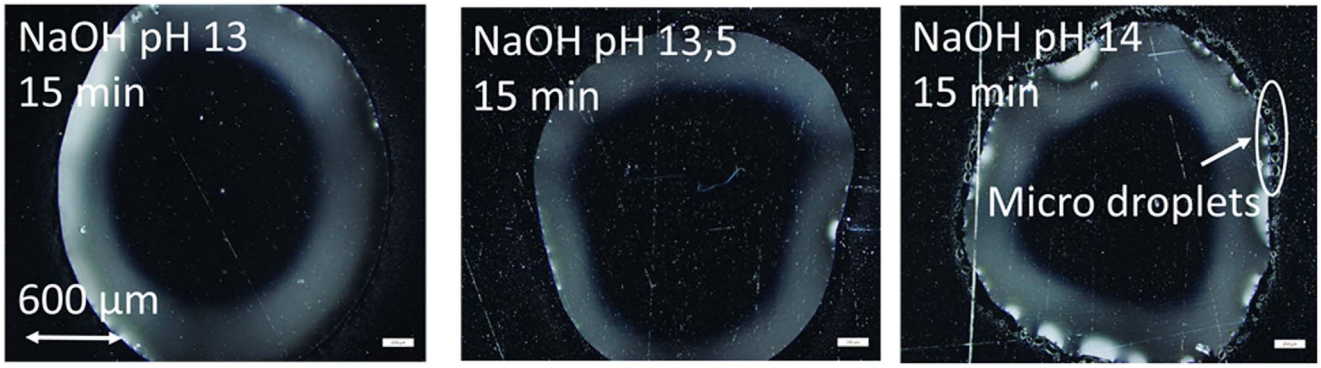

Figure 4. Optical microscopy images of three 0.5 µl droplets from NaOH solution with pH 13, pH 13.5 and pH 14 at room temperature and 95% RH on polished steel, 15 min after droplet application.

dispersive X-ray spectrometer (Quantax XFlash6/60, Bruker Nano GmbH). The acceleration voltage is 15 kV, the resolution is 3 nm and the pressure in the sample chamber is $<10^{-4}$ Pa.

Results

Secondary spreading with NaOH solution on steel.—Figure 4 shows a comparison of three 0.5 µl droplets of NaOH solution with pH 13, pH 13.5 and pH 14 on polished DC01 steel at 95% RH and room temperature, 15 min after droplet application. 5 samples per solution were studied, all of which showed the same qualitative results. 15 min after droplet application, the droplets with NaOH solution of pH 14 show the micro droplets, which grow with time and are typical of secondary spreading. At pH = 13.5, micro droplets also form initially, but recede over time (Fig. 5). The droplet probably becomes less alkaline due to the absorption of CO_2 from the air ($2NaOH + CO_2 \rightarrow Na_2CO_3 + H_2O$). If the observed micro droplets are indeed due to secondary spreading, there is a critical pH of 13.5 on the steel used at 95% RH and room temperature from which secondary spreading begins.

It is typical for secondary spreading in air that the micro droplets contain carbonates.[1,4,8,10,11] Therefore, the composition of the micro droplets is analyzed by SEM and EDX. One 0.5 µl droplet of NaOH solution with pH 14 is dried out at room climate (44.9% RH, 21.3 °C) under the microscope after 2 h of storage at 95% RH and room temperature. Afterwards the sample is stored above silica gel and

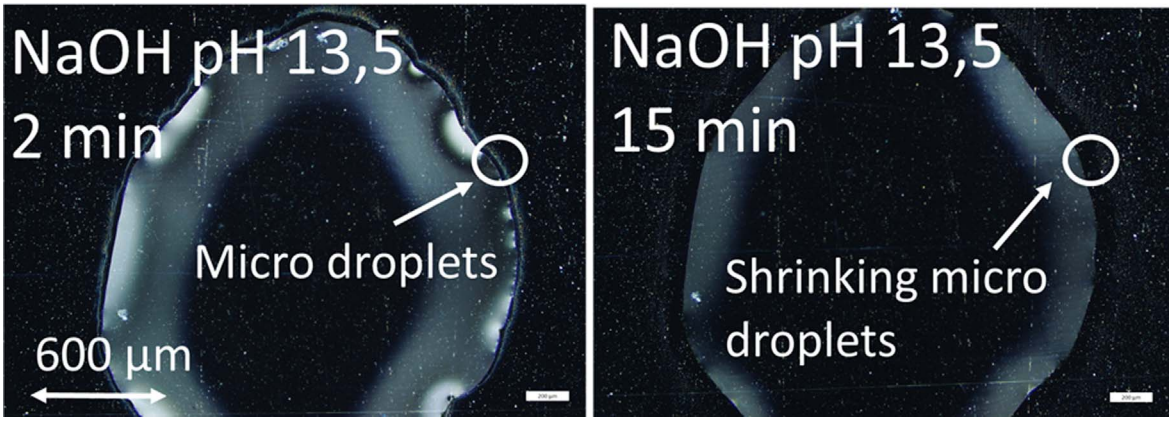

Figure 5. Optical microscopy images of a 0.5 µl droplet of NaOH solution with pH 13.5, 2 min and 15 min after droplet application on polished steel at room temperature and 95% RH.

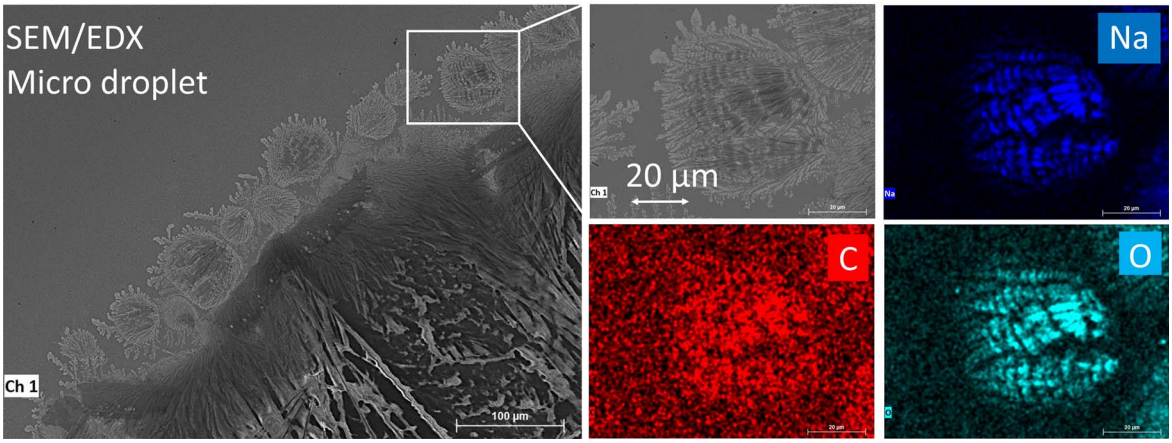

Figure 6. The EDX mapping shows Na, O and C in a micro droplet, which suggests Na_2CO_3.

then examined by SEM/EDX on the same day. Figure 6 shows a SEM image of an edge section of the dried droplet with a selected micro droplet from which a 2-dimensional elemental distribution is recorded by the EDX, so called EDX-mapping. EDX mappings of two other micro droplets are also conducted, which are not shown here. In all three micro droplets investigated, EDX mapping reveals common accumulations of sodium Na, carbon C and oxygen O, indicating sodium carbonate. Sodium carbonate is formed by the reaction of NaOH with CO_2 from the air and, in contrast to NaOH, can crystallize at 45% RH (critical RH of $Na_2CO_3{\cdot}10\ H_2O$: 87% RH at 24.5 °C[24] vs critical RH of $NaOH \cdot H_2O$: 6% RH at 25 °C[25]). The composition of the deposits suggests that micro droplets around droplets of NaOH solutions are products of secondary spreading.

No evidence of corrosion was observed in any tests with NaOH solution drops. This was to be expected, as iron is passive in alkaline solutions. At very high pH values, however, iron could dissolve into solution as a ferrate. Nevertheless, due to the low droplet volume, a high oxygen concentration is to be expected, which favors the passivation of the steel. The dissolution of the iron would lead to the removal of the substrate and thus to roughening, as well as to the formation and possible precipitation of corrosion products. A roughening of the substrate would be visible under the microscope by a higher brightness, the formation and precipitation of corrosion products as clouding of the electrolyte. None of these were observed.

From these investigations it can be concluded that secondary spreading is also possible with droplets of NaOH solution on steel without corrosion and without external cathodic polarization. No corrosion or cathodic polarization under the droplets is necessary for secondary spreading, the high pH value is sufficient. The connection with corrosion or cathodic polarization is secondary. The cathodic partial reaction of oxygen reduction causes alkalization at the edge of the droplet and this in turn causes secondary spreading. Even if corrosion is not absolutely necessary, it is still conceivable that corrosion contributes to secondary spreading. It is very interesting that a limit of the pH value was found above which secondary spreading begins. The critical pH for the steel used at 95% RH and room temperature is 13.5.

In a preliminary experiment, it was observed that secondary spreading at 95% RH and room temperature on polished DC01 steel only occurs with 100 µl droplets of 0.171 M NaCl solution, but not with solutions of the same molar concentration containing $MgCl_2$, $CaCl_2$, NH_4Cl, $(NH_4)_2SO_4$, NH_4NO_3 or NH_4HSO_4, although corrosion has been observed. This is consistent with the results of Tsuru et al. and Zhang et al. Both found no secondary spreading of droplets from $MgCl_2$ solution on low-alloy steel and Zhang et al. also found no secondary spreading with droplets from $CaCl_2$ solution. In both studies, however, secondary spreading was observed with droplets of NaCl and KCl solution, by Zhang additionally with LiCl solution.[3,6]

In the following, it will be estimated whether the critical pH value of pH 13.5 for secondary spreading on DC01 steel can be achieved with the cations Na^+, NH_4^+, Mg^{2+}, Ca^{2+}, Li^+ and K^+. The maximum pH value at the droplet edge is that of the saturated solution of the respective hydroxide, as this would precipitate at a higher concentration and thus no longer contribute to the pH value. In case of NH_4^+, NH_3 forms with OH^-.

It is assumed that the activity is equal to the concentration. Depending on the degree of protolysis α, the pH value of a hydroxide solution can be calculated approximately with a maximum error of 0.2 pH units using the following relationships:[22]

$$\text{For } c_{Base} \leqslant K_B,\ \alpha \geqslant 0{,}62 \quad pH = 14 + \log c_{Base} \qquad [4]$$

$$\text{For } c_{Base} \geqslant K_B,\quad \alpha \leqslant 0{,}62 \quad pH = 14 - \frac{1}{2}(pK_B - \log c_{Base}) \qquad [5]$$

- K_B = base constant, pK_B = base exponent/-
- α = degree of protolysis/-
- c_{Base} = molar concentration of the base/mol/l

The values of the saturation concentration of the base and the pH value of a saturated hydroxide solution calculated from the solubility are shown in Table II. The critical value for secondary spreading of pH 13.5 is only reached by the hydroxides of the cations Na^+, Li^+ and K^+, with which secondary spreading was also observed. Hydroxides from Ca^{2+} and Mg^{2+} and NH_3 do not reach this value. For NH_3, the maximum pH value is probably even lower than calculated, as NH_3 is gaseous and evaporates.

Whether secondary spreading with a cation takes place on the steel used depends on whether the critical pH value of 13.5 is reached by the hydroxide formed at the edge of the droplet.

Table II. Solubility and pH value of the saturated hydroxide solution pH_{max}.

Dissolved substance	Solubility/ g/l H_2O	Molar mass/ g/mol	Molare solubility/ mol/l H_2O	pK_B/-	pH_{max}/-
NH_3	609	17	36[a)]	4,8[d)]	12,4
$Ca(OH)_2$	1,6	74	0,02[b)]	1,4[d)]	12,3
$Mg(OH)_2$	0,01	58	0,0002[c)]	2,6[d)]	10,2
NaOH	1000[d)]	40	25	-0,8[d)]	**15,1**
LiOH	124[d)]	24	5	0,2[d)]	**14,3**
KOH	1207[d)]	56	22	-0,7[e)]	**15,0**

a) [26], 20 °C, b) [27], 25 °C, c) [28], 22 °C, d) [25], 25 °C, e) [29], 25 °C.

Growth rates of micro droplets and spreading zone with Na cations.— *Growth rate of the spreading zone* m_{SP}.—100 µl droplets of 1% NaCl solution are applied at 95% RH and room temperature to polished steel (standard, soft annealed, normalized and large-grain annealed) and to pure iron and microscoped for 2 h. One drop was analyzed per solution/substrate combination, a second sample was analyzed for 1% NaCl solution on standard steel.

After 2 h of observation, images are also taken of four other areas at the edge of the droplet. The width of the spreading zone W_{SP} and the diameter of the largest micro droplets L_M are measured threefold from the microscopy images. The growth laws of the spreading zone and the micro droplets emerge from the two-hour observation of a droplet area. With knowledge of the growth laws, the average values for the entire droplet can be determined from the four images of other droplet areas, taken after two hours.

The use of 1% NaCl solution has the disadvantage that the pH value at the edge of the droplet is not defined. If there are differences in the appearance of the secondary spreading, these differences could stem directly from influences of the substrate on the secondary spreading or indirectly from influences of the substrate on the corrosion and thus on the pH value.

In order to eliminate the influence of the substrate on the corrosion and thus on the pH value at the edge of the droplet, additional experiments are carried out with 1 molar NaOH solution instead of 1% NaCl solution. As already shown, secondary spreading takes place even without active corrosion. A very high pH value e.g. pH 13.5 for DC01 steel is sufficient. Differences in the behavior of the spreading zone are therefore directly attributable to the properties of the substrate and not to differences in the pH value. In order to work out the influence of the NaOH concentration, droplets on standard steel from 1 molar to 8 molar NaOH solution are also examined.

After droplet application, the contact angle of the droplets from NaCl solution and also from NaOH solution decreases and the droplets become wider, while the contact line moves outwards. In this phase, the primary droplets can swallow parts of the spreading zone and micro droplets, which distorts the determination of the growth rates of the spreading zone and the micro droplets to lower values. Therefore, the values for the spreading zone and micro droplets are only used after the movement of the contact line came to a standstill. On average, the contact line is pinned after 10 min and the micro droplets and the spreading zone can then grow largely undisturbed. Occasional subsequent widening of the droplet can be recognized by sudden reductions in the size of the spreading zone and the micro droplets. One example is the curve for the NaCl droplet on normalized steel shown in part a) of Fig. 7, which was divided into a part before and a part after the sudden movement of the contact line ("jump"). Further disturbances can occur at very high spreading rates, when an extensive spreading zone has already formed before the primary droplet comes to a complete standstill. This can be seen in part c) of Fig. 7 for a droplet from 1 M NaOH solution. The error-prone values are marked with white-filled measuring points. For the determination of the growth rates, the described faulty areas are not used.

In Fig. 7, the width of the spreading zone is plotted against the root of the time after the standstill of the primary droplet for

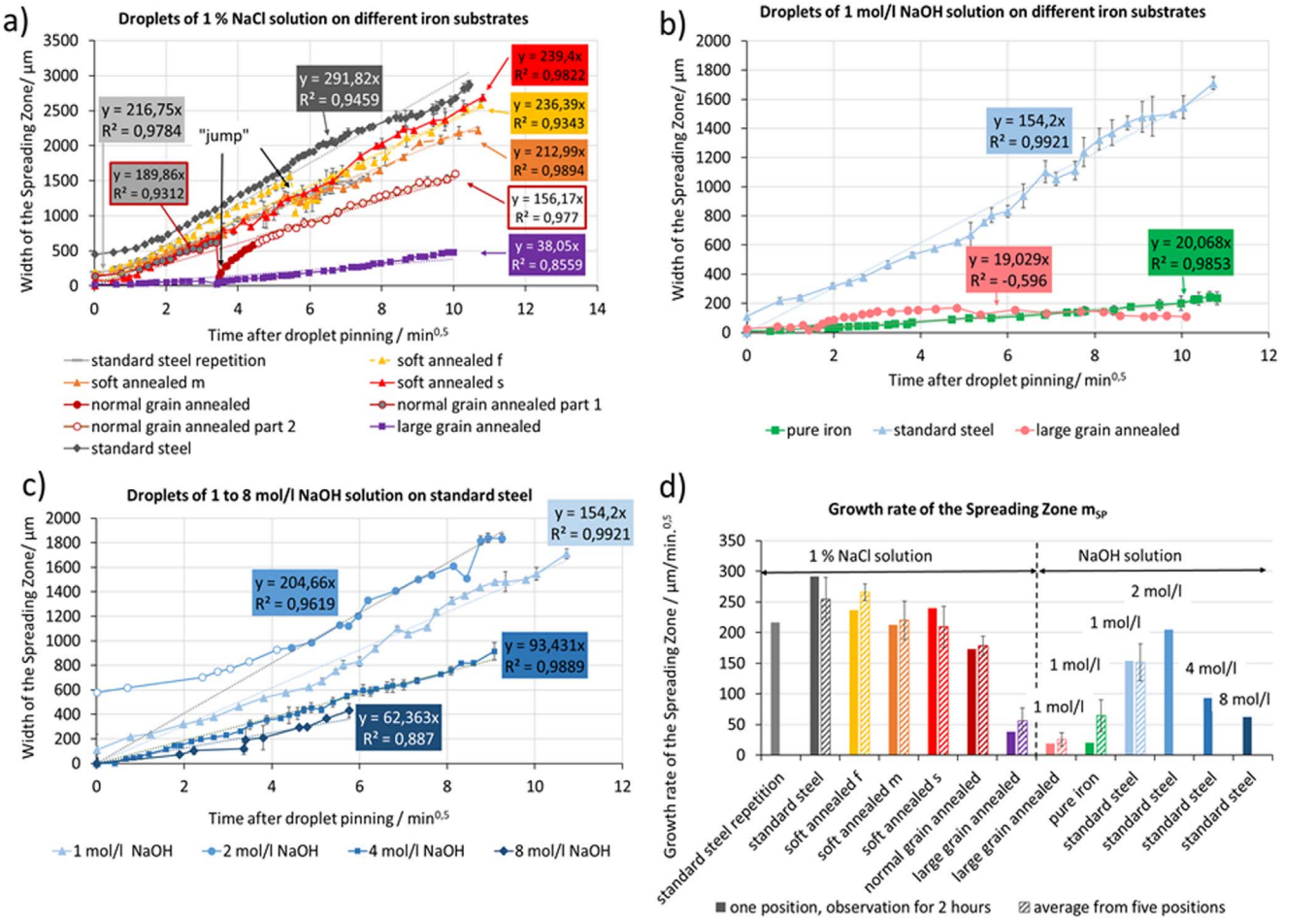

Figure 7. Width of the spreading zone W_{SP} vs the square root of time for 100 µl droplets (a) from 1% NaCl solution on different substrates, (b) from 1 mol/l NaOH solution on different substrates and (c) from 1 to 8 mol/l NaOH solution on DC 01 standard steel. Part (d) compares the values of the spreading velocities m_{SP} from the observation of one droplet section with the averaged values from five positions at the edge of the droplet.

Table III. Growth rate of the spreading zone m_{SP} determined from one area at the droplet edge and from five areas of the droplet edge assuming a √t-dependence.

		m_{SP} from one area at the droplet /μm/min$^{0.5}$		Mean $_{mSP}$ from five areas at the droplet edge m_{SP}/ μm/min$^{0.5}$	
Substrate	Solution	Value	Correlation coefficient R^2	Mean value	Single standard deviation
Standard steel	1% NaCl	217	0,98	255	36
Standard steel repetition	1% NaCl	292	0,95	—	—
Soft annealed f	1% NaCl	236	0,93	266	14
Soft annealed m	1% NaCl	213	0,99	220	31
Soft annealed s	1% NaCl	239	0,98	209	34
Normal grain annealed	1% NaCl	173	0,93/0,98	179	15
Large grain annealed	1% NaCl	38	0,86	56	21
Large grain annealed	1 molar NaOH	19	-0,60	26	11
Pure iron	1 molar NaOH	20	0,99	64	26
Standard steel	1 molar NaOH	154	0,99	151	30
Standard steel	2 molar NaOH	205	0,96	—	—
Standard steel	4 molar NaOH	93	0,99	—	—
Standard steel	8 molar NaOH	62	0,89	—	—

different combinations of electrolyte and substrate. All but two curves show a high correlation coefficient of the fitted straight line of well over 0.93. The determined values of the spreading rate m_{SP} are also listed in Table III. The growth of the spreading zone can be described by the following relationship:

$$W_{SP} = m_{SP}\sqrt{t} \quad [6]$$

- W_{SP} = Width of the spreading zone/μm
- m_{SP} = Growth coefficient (corresponds to the gradient of the equalization line through the origin in Fig. 7)/μm/s$^{0.5}$
- t = Time after standstill of the contact line/s

Part a) of Fig. 7 shows the growth of the spreading zone of droplets of 1% NaCl solution on steels with different heat treatments. There is no significant difference in the growth rate of the spreading zone m_{SP} of NaCl droplets on standard steel compared to that on soft-annealed steel. All values of m_{SP} are within the difference of the two measurements on standard steel except for negligibly small deviations. m_{SP} on standard and soft-annealed steel varies from 213 to 292 μm/min$^{0.5}$. m_{SP} on normalized steel, on the other hand, is lower at 152 to 190 μm /min$^{0.5}$ and m_{SP} on large-grain annealed steel is significantly lower than m_{SP} on standard or soft-annealed steel at only 38 μm/min$^{0.5}$. The heat treatment can strongly influence m_{SP}. It remains to be seen what exactly changed m_{SP}. As already mentioned, the substrate could directly influence m_{SP} via changes in the microstructure or the changes in the microstructure change the corrosion rate and thus influence the pH value at the edge of the droplet. On pure iron, corrosion was inhibited to such an extent that no secondary spreading took place with NaCl solution. However, the experiments with 1 molar NaOH solution in Part b) in Fig. 7 show, that secondary spreading is also possible on pure iron.

From Part b) in Fig. 7 also the spreading rates m_{SP} for droplets of 1 molar NaOH solution on standard steel, large-grain annealed steel and pure iron are calculated. The NaOH concentration is identical for all three samples and differences in the spreading rate m_{SP} are directly dependent on the substrate. m_{SP} is almost identical and very low at 19 and 20 μm/min$^{0.5}$ on coarse annealed steel and pure iron, while it is much faster on standard steel with 154 μm/min$^{0.5}$. This fits with the results of Risteen et al., according to which the spreading zone of droplets from NaCl solution is wider on low carbon steel than on pure iron.[13] The steel microstructure therefore has a direct influence on the spreading rate. From the results in Fig. 7, it is not possible to say which properties of the microstructure determine the spreading rate. However, a comparison of the microstructures allows assumptions to be made. The practically identical spreading rate m_{SP} on large-grain annealed steel and pure iron indicates that the differences found in the microstructure between large-grain annealed steel and pure iron, the large pearlite grains have no influence on the rate of spreading. In contrast, the spreading rate on standard steel with numerous small cementite fragments is significantly increased. Based on these results, it is assumed that the rate of spreading depends on the content of defects in the steel substrate. The numerous cementite fragments could possibly result in local disturbances of the growing oxide layer. Differences in the lattice structure could influence the surface energy of the oxide layer and thus have an effect on the rate of spreading.

Part c) in Fig. 7 shows the dependence of the spreading rate m_{SP} on standard steel on the NaOH concentration. As the NaOH concentration increases, the spreading rate m_{SP} also increases. It reaches its maximum at 205 μm/min$^{0.5}$ with 2 molar NaOH and decreases again at higher concentrations.

With NaCl solution, slightly higher values of m_{SP} between 213 and 292 μm/min$^{0.5}$ are achieved. This could be explained if the maximum is not exactly at 2 mol/l NaOH in the bulk electrolyte, but between 1 and 2 or 2 and 4 mol l^{-1}. Further experiments with smaller pH intervals are planned to verify this.

It should be noted that the NaOH concentration in the spreading zone may be lower than in the droplet interior due to the high surface area and the resulting accelerated adsorption of CO_2 from the atmosphere. The local distribution of the NaOH concentration in the spreading zone could also be somewhat different with NaOH droplets than with NaCl droplets. In the former case, fresh NaOH-rich solution can only flow into the spreading zone from the edge of the droplet, whereas with NaCl droplets there is an active cathode that can supply OH^- throughout the spreading zone by reducing oxygen. This does not change the qualitative finding that the NaOH concentration influences the spreading rate m_{SP} and that there is an optimum NaOH concentration at which the spreading rate m_{SP} is maximized.

Part d) in Fig. 7 compares the spreading velocities mSP, which were determined from the 2 h observation of a droplet section, with the averaged values from microscopy images after 2 h of droplet lifetime on 5 different edge sections of the droplets. The values are also shown in Table III. For the droplets from 2 to 8 mol l^{-1} NaOH solution, the spreading rate m_{SP} was not calculated from the images after 2 h, as these droplets still spread considerably after 20 min and it is not clear at which time almost undisturbed growth can be assumed.

Growth rate of micro droplets m_M.—The growth of the mean micro droplet size after standstill of the primary droplet for 100 μl

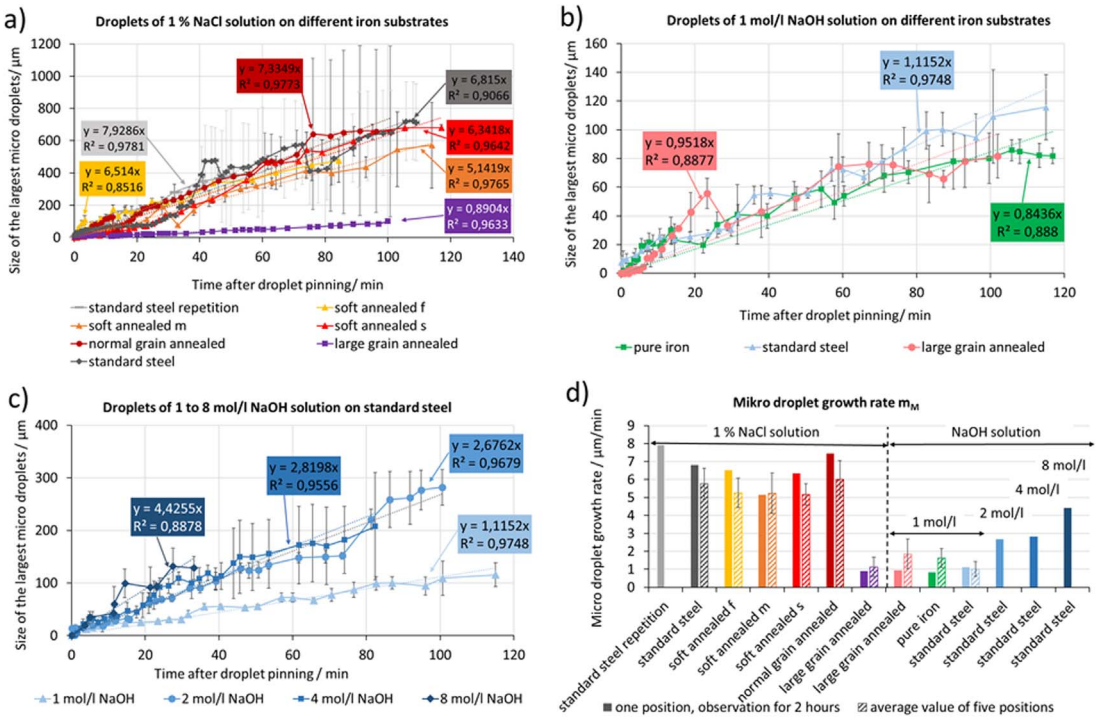

Figure 8. Mean length of the three largest micro droplets L_M vs the square root of time for 100 µl droplets (a) from 1% NaCl solution on different substrates, (b) from 1 mol/l NaOH solution on different substrates and (c) from 1 to 8 mol/l NaOH solution on DC 01 standard steel. Figure (d) compares the growth rate of the micro droplets m_M from the observation of a droplet section with the averaged values of 5 positions at the edge of the droplet.

droplets of NaCl and NaOH solution on different substrates is shown in Fig. 8. The determined values of the spreading rate m_{SP} are also listed in Table IV. A straight line of origin can generally approximate the growth of the mean micro droplet size:

$$L_M = m_M t \quad [7]$$

- L_M = Average size of the three largest micro droplets/µm
- m_M = Average growth rate of the three largest micro droplets/ µm/s
- t = Time after standstill of the contact line/s

Micro droplets grow not only individually, but also by connecting neighboring micro droplets. This becomes more pronounced the larger the micro droplets are. Growth by connecting two micro droplets leads to a sudden increase in droplet size, which is reflected in the high standard deviation of the mean size of the three largest micro droplets L_M. The very high standard deviations for large droplet sizes and also the lower correlation coefficients of 0.85 to 0.98 compared to the measurements of the spreading rate m_{SP} are not a sign of a highly erroneous measurement of the droplet size, but rather reflect the growth behavior of the micro droplets.

In part a) in Fig. 8 no difference in the growth rates m_M of the micro droplets on standard steel, soft-annealed steel and normalized steel with NaCl droplets can be determined. The growth rates range from 5.1 to 7.9 µm min^{-1}. However, a significantly lower growth rate of only 0.9 µm min^{-1} was observed on large-grain annealed steel. The growth of the micro droplets can be altered by annealing of the steel. In principle, the same possibilities as for the growth of the spreading zone can be named as reasons for the different growth of the micro droplets on the different substrates. The question arises

Table IV. Growth rate of the micro droplets m_M determined from one area at the droplet edge and from fife areas of the droplet edge.

		m_M from one area at the droplet edge/µm/min		Mean m_M from fife areas at the droplet edge/µm/min	
Substrate	Solution	Value	Correlation coefficient R^2	Mean value	Single standard deviation
Standard steel	1% NaCl	7,9	0,98	—	—
Standard steel repetition	1% NaCl	6,8	0,91	5,8	0,9
Soft annealed f	1% NaCl	6,5	0,85	5,3	0,8
Soft annealed m	1% NaCl	5,1	0,98	5,2	1,1
Soft annealed s	1% NaCl	6,3	0,96	5,2	0,6
Normal grain annealed	1% NaCl	7,4	0,98	6,0	1,0
Large grain annealed	1% NaCl	0,9	0,96	1,1	0,5
Large grain annealed	1 molar NaOH	1,0	0,89	1,9	0,8
Pure iron	1 molar NaOH	0,8	0,89	1,6	0,5
Standard steel	1 molar NaOH	1,1	0,97	1,0	0,4
Standard steel	2 molar NaOH	2,7	0,97	—	—
Standard steel	4 molar NaOH	2,8	0,96	—	—
Standard steel	8 molar NaOH	4,4	0,89	—	—

Table V. Average size of the spreading zone L_{SP} after 2 h droplet lifetime and average growth rate of the spreading zone m_{SP}. The mean values with single standard deviations from measurements at 5 locations on the droplet are shown in each case. The mean value of 110 min. was used as the time after droplet standstill.

	Width of the spreading zone L_{SP} after 2 h/µm		Mean growth rate of the spreading zone m_{SP}/µm/min^{0,5}		
Electrolyte	Mean	Deviation	Mean	Deviation	Diffusion coefficient of the cation D for infinitive dilution at 25 °C/cm^2/s [25] *
KOH	2767	538	264	49	1,96
NaOH	1593	317	152	30	1,33
LiOH	811	251	77	23	1,03
LiOH Repetition	562	159	54	15	1,03

as to the direct influences of the substrate on the micro droplet growth and the indirect influences on the cathodic activity or the pH value at the edge of the droplet.

Figure 8b shows the growth of the micro droplets starting from a 1 molar NaOH droplet on pure iron, standard steel and large-grain annealed steel. In contrast to the growth of the spreading zone, there is no dependence of the micro droplet growth on the substrate.

Figure 8c shows the growth of micro droplets on standard steel with primary droplets of 1 molar to 8 molar NaOH solution. The growth rate of the micro droplets depends only on the NaOH concentration and not on the substrate.

Assuming that Eq. 7 is generally valid, i.e. $L_m \sim t$, the mean m_M-values were calculated from five different sections of the droplet edge.

In section d), the growth rates of the micro droplets m_M, which were determined from the 2 h observation of a droplet section, are compared with the averaged values from microscopy images after 2 h of droplet life on five different edge sections of the droplets. The calculation is performed analogously to the calculation of the averaged spreading rate by converting Eq. 7 to m_M. The time for almost undisturbed growth is also 110 min. The averaged values for the 2–8 mol l^{-1} NaOH droplets are missing for the reasons already described. The use of the averaged values does not change the dependencies found.

Growth rate of the spreading zone with potassium and lithium cations.—The measurement of the spreading rate m_{SP}, already described in a previous chapter shows a $\sqrt{t}$ -dependence. A $\sqrt{t}$-dependence hints a transport-controlled rate-determining step.[30] This step could probably be the diffusion or migration of cations or a combination of both. Diffusion as well as migration often show a square root of time dependence.[31] If the diffusion of cations through a possibly existing thin electrolyte film in the spreading zone plays a role for secondary spreading, a dependence of the spreading rate on the diffusion coefficient of the cation in aqueous solution should be evident. Therefore, the rate of spreading was determined in the same way as in the previous chapter for droplets of 1 molar LiOH and 1 molar KOH on standard steel and compared with the rate of spreading of droplets of 1 molar NaOH. A repeat measurement was made with LiOH. The results are summarized in Table V. Figure 9 left shows the growth of the spreading zones during 2 h droplet lifetime on one droplet section.

The spreading zone also widens with LiOH and KOH according to a $\sqrt{t}$-law, as shown in Fig. 9 on the left side. On the right-hand side of Fig. 9, the averaged spreading rate from 5 droplet sections were plotted against the diffusion coefficient of the respective cations. The spreading rate increases with the diffusion coefficient. The data are not sufficient to determine whether this is a linear relationship, as the good correlation suggests. A contribution of migration to cation transport cannot be excluded.

Is there a thin electrolyte film between the micro droplets?.—As already described in the introduction, it is unclear how the micro droplets are formed and how the salts they contain get into the micro droplets. One theory is that a thin film of liquid connects the micro droplets with the primary droplet. However, this possibility raises the question of how the micro droplets and the primary droplet retain their shape. Alternatively, the micro droplets could be separated from each other by non-wetted areas. In order to still allow the transport of ions, one could assume thin connecting paths between

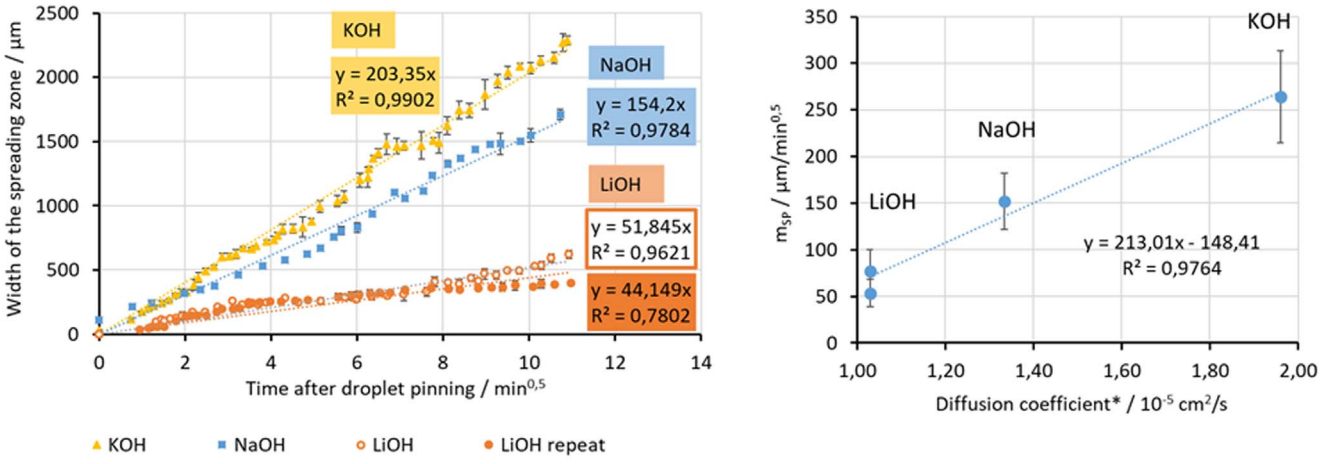

Figure 9. Left: Growth of the spreading zone with 100 µl droplets of 1 molar KOH, NaOH and LiOH solution during 2 h, measured at one section of the edge of a droplet. Right: Correlation of the mean spreading rate m_{SP}, from measurements on 5 droplet sections with the diffusion coefficient of the respective cation from Table V.

the micro droplets. This would be possible if a heterogeneous substrate with hydrophilic and hydrophobic areas is assumed. Micro droplets could grow on large hydrophilic regions and thin elongated hydrophilic regions could act as connecting pathways that enable ion transport between primary droplets and micro droplets. Hydrophobic areas, on the other hand, could separate the micro droplets from the primary droplet. This could create a network of electrolyte reservoirs (micro droplets) and connecting pathways. This assumption seems justified for steel with its complex structure of ferrite grains of different orientation, a distributed cementite phase, grain boundaries and precipitates. It is assumed that these defects in the substrate also cause the oxide layer to become richer in defects, so that a surface with heterogeneous surface energy is formed even if the surface is covered with a thin oxide film, as is to be expected with passive steel. Contamination of the surface could also contribute to this heterogeneity.

If this theory were correct, the micro droplets would represent the structure of the steel. One would then expect particularly small and finely distributed micro droplets to be formed on standard steel and soft-annealed steel with a small grain size, while large and widely spaced micro droplets would tend to form on large-grain annealed steel due to the large grain size. However, this was not observed. Instead, very small micro droplets form close together at the beginning, independent of the substrate. On large-grain annealed steel, the younger micro droplets are even smaller than the grain size of the steel, as a comparison of the spreading zone with the etched microstructure in Fig. 10 shows. Micro droplets can therefore also form on undisturbed grains and do not reflect the structure of the steel. It is therefore also unlikely that there are connecting paths between the micro droplets that supply them with solution. In contrast there seems to be a thin film of liquid connecting the micro droplets.

This theory is supported by SEM/EDX images of a 100 µl NaCl droplet on standard steel, which corroded at 50% RH and 25 °C for 48 h and was then dried quickly in a nitrogen stream. SEM images of the spreading zone at different magnifications are shown in Fig. 11, a dried micro droplet in Fig. 12. A second micro droplet, which is not shown here, was also examined with SEM/EDX and produced qualitatively identical results.

Dried micro droplets leave behind two types of deposits: There are polygonal deposits, which appear light in the SEM images, and needle-like deposits, which appear dark in the SEM images. Larger deposits are found within dried out micro droplets, whose former outline can be recognized by circularly arranged bright fine deposits. Larger dark needle-shaped deposits can also be found on the wetting front. The light and dark deposits could be two different compounds crystallized from the former spreading zone. This is suggested not only by the different crystal shapes, but also by the brightness of the deposits in the SEM images. In the SEM image with EDX-mapping of a dried out micro droplet in Fig. 12, it can be seen, that the bright polygonal deposits are NaCl crystals and the dark needle-shapes deposits are a compound of sodium, carbon and oxygen, which is most likely sodium carbonate. Sodium carbonate has already been found by other authors within the spreading zone of NaCl droplets.[1,8,11]

Remarkably, the SEM images also show evenly distributed bright deposits between the micro droplets, which could originate from a thin, dried-out electrolyte film containing salt. Unfortunately, the deposits are too small to determine their composition with EDX, but the crystal form and the brightness suggests NaCl. In addition to the topography, the sample material also contributes to the contrast in the secondary electron mode used.[32] There exists a homogeneous darker layer on which the fine bright dot-like deposits rest. This layer is best seen at the wetting front in comparison to the non-wetted steel substrate. This dark layer could possibly consist of sodium carbonate, because the brightness fits to the brightness of the darker needle-like deposits, consisting of Na, O and C (see Figs. 11 and 12). The described observations could be explained by the theory that during secondary spreading of a NaCl droplet, a thin electrolyte film containing NaOH spreads outwards from the edge of the droplet. This strongly alkaline film absorbs CO_2 from the air and forms Na_2CO_3. This appears as a dark layer in the SEM images. When micro droplets form, these also contain NaOH and form Na_2CO_3, which crystallizes out more slowly during drying than that in the thin film and thus forms larger crystals. Cl^- could also diffuse into the spreading zone from the edge of the droplet. NaCl then forms as it dries out. Diffusion from the edge of the droplet would explain why there are more bright deposits near the primary droplet than near the wetting front.

With the data available so far, only an estimate of the plausibility of both hypotheses, the connecting paths between micro droplet due to inhomogenouse wetting an the connicting liquid film between micro droplets can be given. Due to the presented data, the thin film hypothesis is therefore considered more plausible than the alternative hypothesis with inhomogenouse wetting. However, none of the hypotheses can be proven or ruled out.

More data on the distribution of the micro droplets and on the local distribution of the surface energy, as well as the influence of the microstructure and the oxide layer on the surface energy would be necessary in order to be able to rule out the alternative hypothesis of inhomogenouse wetting with certainty. It would also be necessary to experimentally prove the film between the microdroplets in situ in

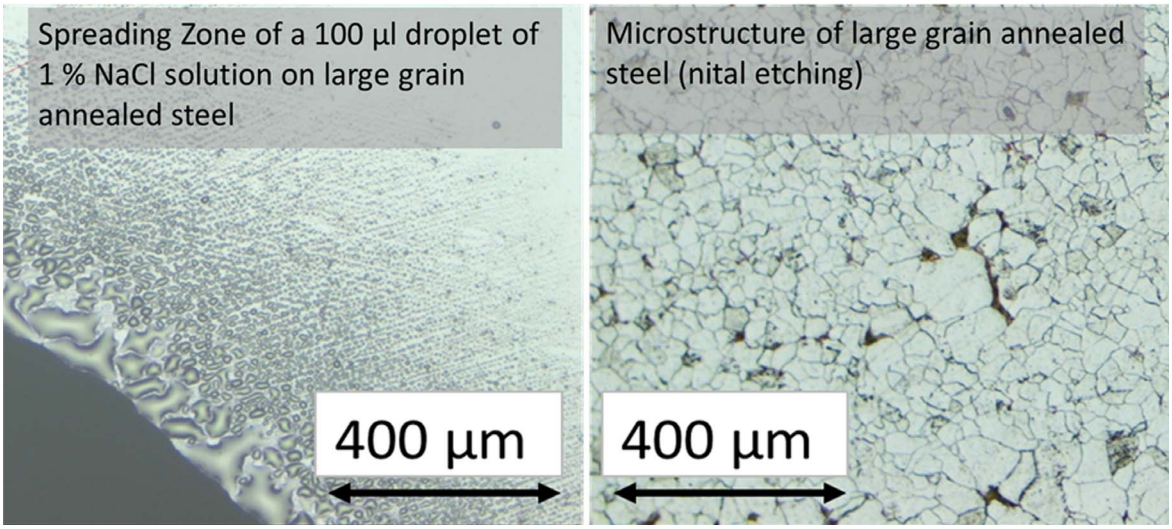

Figure 10. Comparison of microscopy images of the spreading zone of a NaCl droplet after 2 h droplet lifetime on large-grain annealed steel with the microstructure of the same substrate.

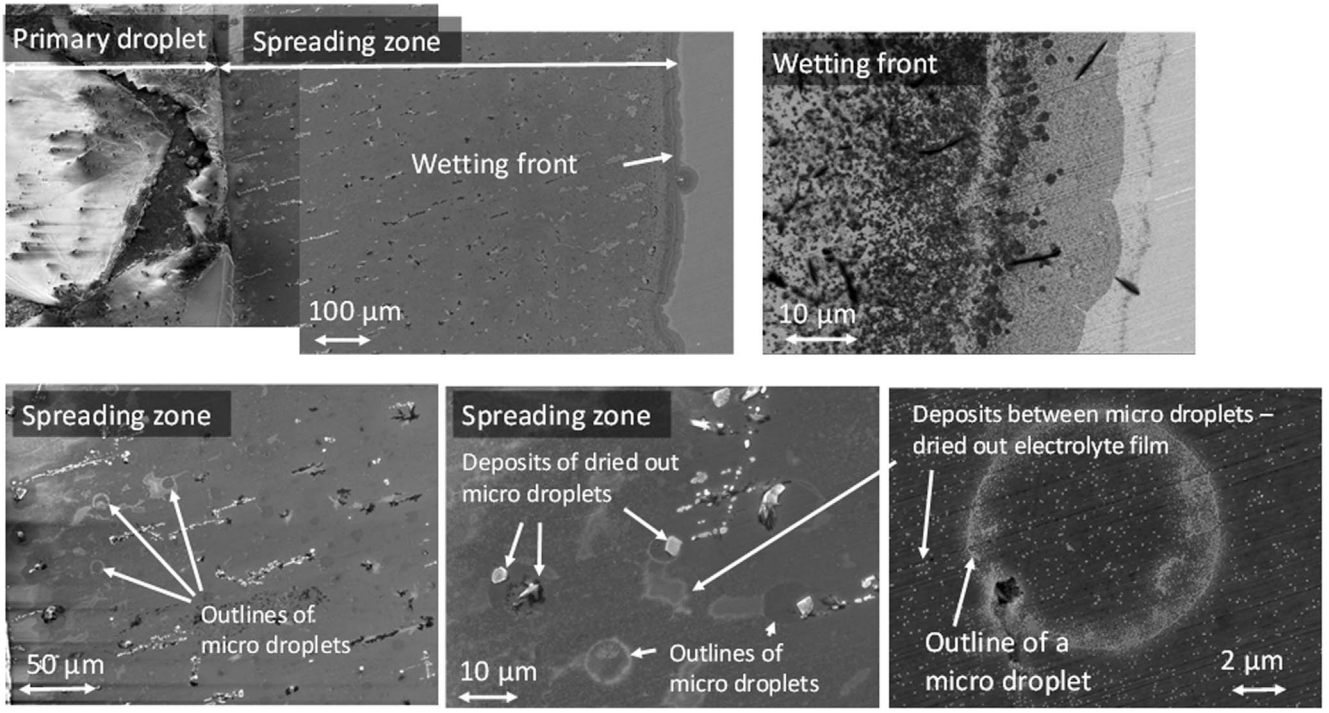

Figure 11. SEM images of standard steel with spreading zone of a 100 µl droplet of 1% NaCl solution after exposure to air at 50% RH and 25 °C for 48 h (secondary electron modus).

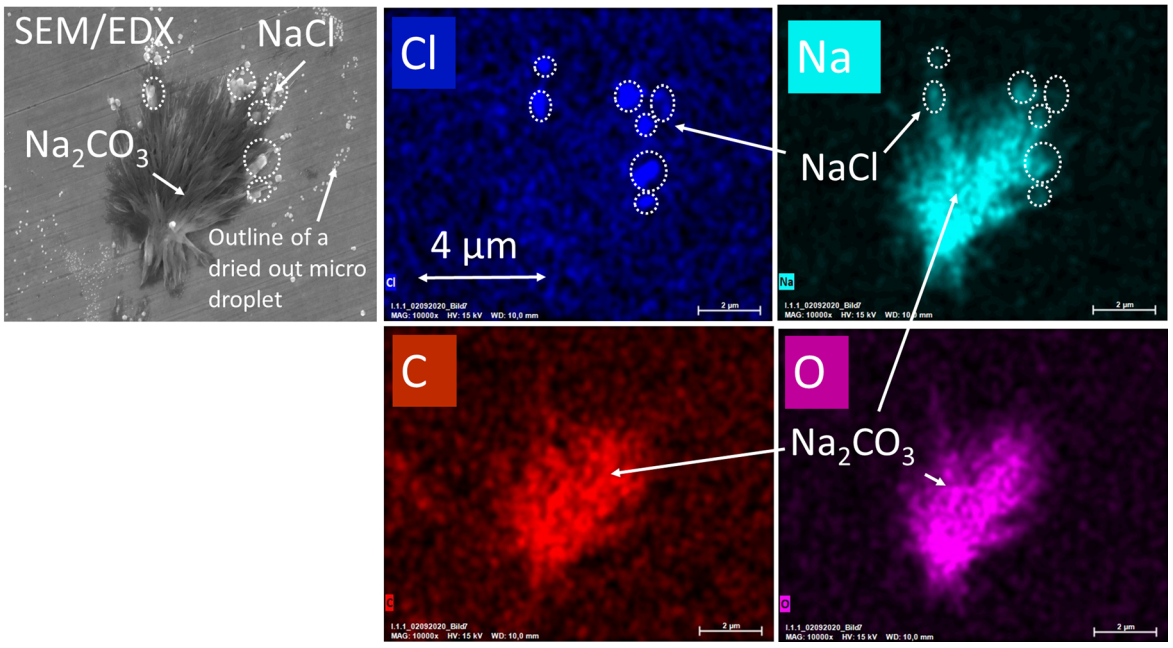

Figure 12. SEM images (secondary electron modus) with EDX mapping of a dried micro droplet.

order to prove the hypothesis of the thin film between the micro droplets beyond doubt.

E_{corr}-profile of the spreading zone of NaCl-droplets on standard steel.—Figure 13 shows E_{corr} potential profiles of a large 100 µl droplet and a small 0.5 µl droplet of 1% NaCl solution on standard steel at 95% RH and 25 °C measured with the Kelvin Probe. During 6 h and 44 min. four potential profiles were recorded consecutively. The large droplet is applied 17 min. before the start of the SKP measurement, the small droplet directly before it is reached by the probe about 10 mm away from the spreading zone of the large droplet. The drying of the droplets can be seen from the height profile. Different areas of the droplet can be identified by different potentials. A comparison with the microscopy images of the droplets directly after the last SKP measurement, which are also shown in Fig. 13, helps here. The anodic area in the center of the droplet is at a uniform low potential. A slight step separates it from the cathode at the edge of the droplet, which has a slightly higher potential. The potential rises directly at the edge of the droplet. This is where the spreading zone (SP) is located. The continuous increase in E_{corr} is typical of the spreading zone. In droplets without secondary spreading, the potential rises almost vertically at the edge of the droplet. The end of the

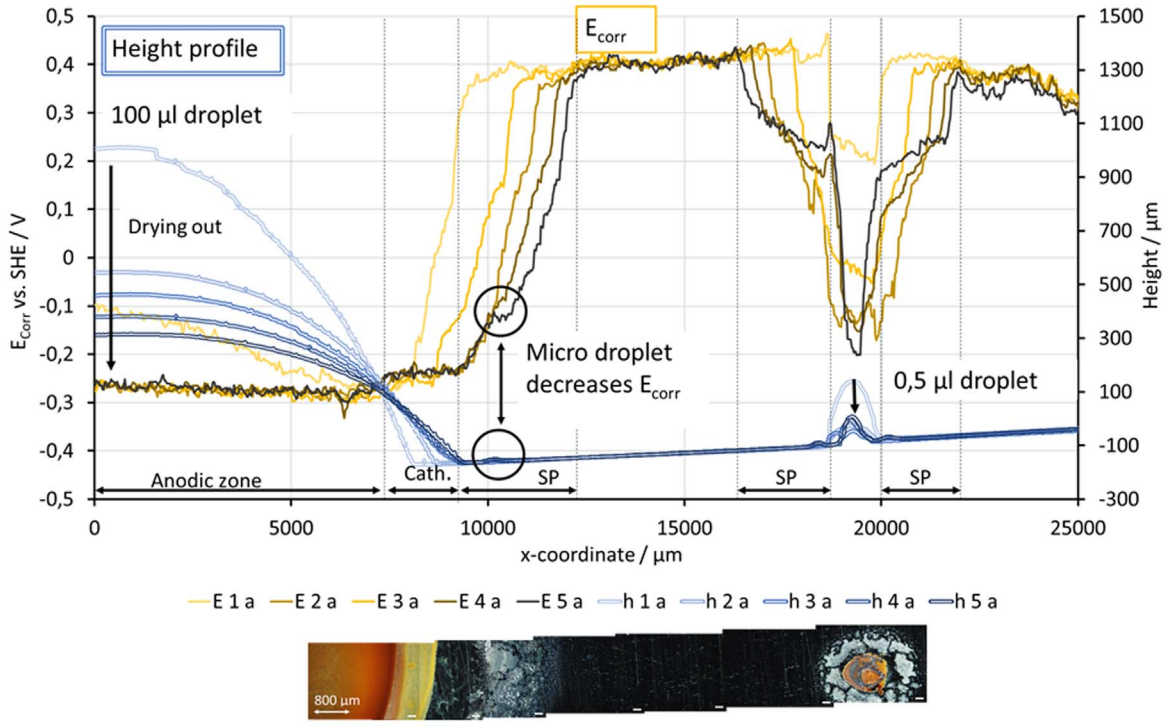

Figure 13. E_{corr} profiles of a large 100 µl and a small 0.5 µl droplet of 1% NaCl solution on standard steel at 25 °C and 95% RH. The scanning direction is always from left to right, starting from the apex of the large droplet. After the fourth line scan, the large droplet is 6 h 44 min. old and the small droplet is 5 h 34 min. old. Below are optical microscopy images of the sample directly after the SKP measurement.

spreading zone is reached when the potential is equal to the potential of the unwetted periphery. A repeat test was carried out, which produced a comparable potential profile, but is not shown here.

Qualitatively similar E_{corr} profiles with low potential below the droplet, increased potential within the spreading zone and high potential in the periphery were measured for droplets of NaCl solution by other research groups on steel,[3] zinc[1] and copper.[11] For comparison, Ecorr-measurements using SKP for droplets without reported secondary spreading can be found in[33] for droplets of $(NH_4)_2SO_4$ solution on zinc and in[3] for droplets of $MgCl_2$ solution on steel.

How the different potentials during secondary spreading can be interpreted, is dealt with in the discussion section.

Discussion

Is secondary spreading a form of pseudo-partial wetting?.—The results of the size comparison of micro droplets and steel structure and the SEM images of the spreading zone of a NaCl droplet on steel suggest the existence of an electrolyte film that connects the micro droplets with each other. This raises the question of how the micro droplets and also the primary droplet can retain their shape and why the primary droplet, micro droplet and electrolyte film do not flow together to form a single flat droplet. One would assume that this significant reduction in the surface area solution/air would make the entire system more energetically favorable.

Secondary spreading does not appear to be explainable with classical wetting theory. Therefore, the theory presented here on the structure of the spreading zone is based on the already known wetting theory of thin films. The basics required to understand this theory are briefly described below.

For liquid films that are thinner than the range of molecular interactions, the surface tension alone is no longer sufficient to describe the free energy of the system: A new energy term P(e) must be added, which describes the interaction between the solid/liquid and liquid/gas interfaces.[34]

The free energy per unit area of a spreading liquid film with thickness e on an ideally smooth and homogeneous solid is:[35]

$$F(e) = \gamma_{SL} + \gamma_{LV} + P(e) \quad [8]$$

- e = Thickness of a spreading liquid film
- F(e) = Free energy (per unit area) of a spreading liquid film with thickness e
- γ_{SL} = Solid/liquid interface energy
- γ_{LV} = Solid/vapor interface energy
- P(e) = Energy term to describe the interaction between the solid/liquid and liquid/gas interfaces

For macroscopic thickness e, P(e) approaches zero. For e greater than the molecular size a_0, P(e) is determined by long-range Van der Wals (VdW) forces:[35]

$$P(e) = \frac{A}{12\pi e^2} a_0 \ll e \ll l \quad [9]$$

- $A = A_{SL} - A_{LL}$ Difference in Hamaker constants (the Hamaker constant describes the VdW interactions of a material and is calculated according to the Lifshitz theory from the dielectric constant of the bulk material and the refractive index (RI)[36])
- l = Limitation in the ultraviolet range

For very small thicknesses e applies:[35]

$$P(e \to 0) = S = \gamma_{SG} - \gamma_{SL} - \gamma_{LV} \quad [10]$$

And therefore:

$$F(e \to 0) = \gamma_{SG} \quad [11]$$

- S = Spreading coefficient
- γ_{SG} = solid/vapor interface energy

For very small film thicknesses e, P(e) includes not only van der Wals forces, but also dipole-dipole interactions and H-bridges, among others.

The spreading behavior of a liquid on a solid can be derived from the progression of the free energy F(e) with the film thickness e. The independent variables A (difference of the Hamaker constants) and S (spreading coefficient) determine the shape of the energy function F (e). Different wetting regimes occur depending on the amount and sign of A and S:[35]

I. Complete wetting: $S > 0$, $A > 0$F(e) is either a continuously decreasing function or has a maximum at $e = e_{max}$. F(e) is greater than γ_{SL}- γ_{LV} for $e \rightarrow 0$. The energy minimum of the function F(e) is at $e \rightarrow \infty$. This results in a thick liquid film on the solid surface.
II. Partial wetting: $S < 0$, $A > 0$ or $A < 0$F(e) is smaller than γ_{SL}- γ_{LV} for $e \rightarrow 0$ and has a maximum or is continuously increasing. In both cases, the energy minimum is at $e \rightarrow 0$, resulting in a droplet surrounded by a dry substrate. The contact angle follows Young's equation.
III. Pseudopartial wetting: $A < 0$, $S > 0$ or $S < 0$

F(e) has a minimum at $e = e_{min}$. This results in a liquid film with the thickness e_{min}. Excess liquid collects in a droplet that is in equilibrium with the liquid film. The contact angle Θ of the droplet in equilibrium with the liquid film is:

$$\gamma_e = \gamma_{LV} \cos \Theta \qquad [12]$$

γ_e is the effective surface energy of the liquid film.

The respective course of the energy function F(e) is shown qualitatively in Fig. 14. The wetting regime of pseudopartial wetting is strongly reminiscent of secondary spreading, in which a large primary droplet is also in equilibrium with a surrounding microscopically thin liquid film in the spreading zone.

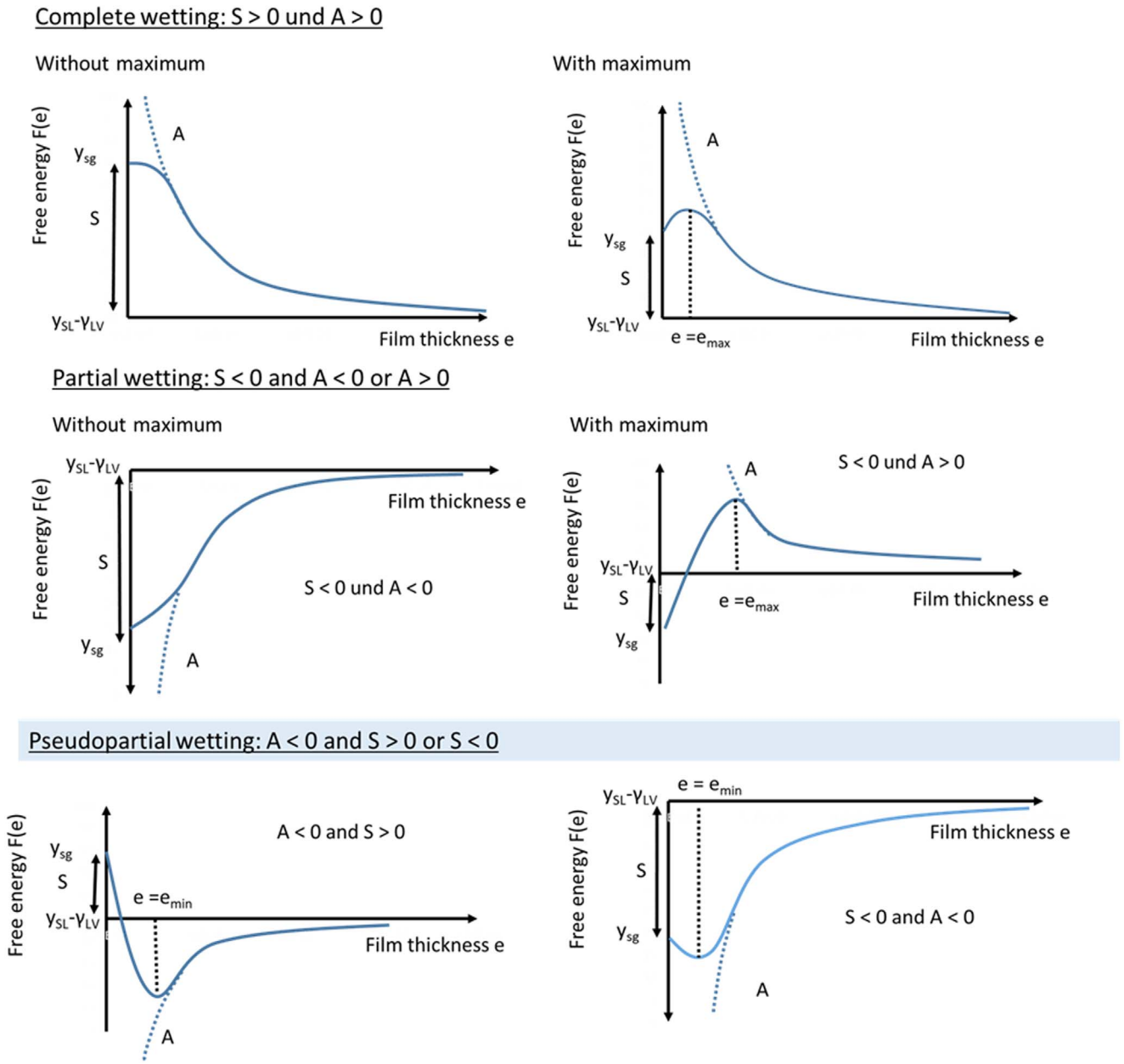

Figure 14. Qualitative course of the function F(e) for the three wetting regimes: complete wetting, partial wetting and pseudo-partial wetting. Self-drawn, based on.[35]

The assumption that secondary spreading is a form of pseudo-partial wetting solves the problem of non-flowing droplets on a liquid film: A macroscopic primary droplet can be stable on a thin liquid film without deliquescing on it. This also applies to micro droplets. Due to the energy minimum of the energy function F(e) at $e = e_{min}$, only a defined film thickness e_{min} is stable in the spreading zone. Excess liquid remains in the primary droplet or collects in micro droplets in the spreading zone.

The considerations described above apply to a droplet in equilibrium. However, if a droplet is applied to a substrate, as in this study, this equilibrium state must first be reached. As we have seen, the primary droplet expands first. After it has come to a standstill, or even before, a liquid film begins to spread outwards in the case of secondary spreading. Such behavior has already been described in the literature. A thin liquid film that spreads from a macroscopic droplet front is called a "precursor film." "Precursor films" occur with complete and pseudo-partial wetting.[37] Popescu et al. gives an overview of the state of knowledge on precursor films. As long as the primary contact line is moving, the film is called an adiabatic film, after the primary contact line has stopped, it is called a diffuse film.[38] Only the case of the diffusive film will be considered in more detail, as the experiments showed that the adiabatic phase lasted only a few minutes or was not visible at all in most of the substrate/solution combinations investigated. Also, the growth rate m_{SP} of the spreading zone could only be determined when the primary droplet was stationary, i.e. in the diffusive phase.

The length of the diffusive film L(t) increases consistent with diffusion laws when the primary contact line comes to a standstill:[38]

$$L(t) \sim \sqrt{D_{film}\, t} \qquad [13]$$

- L(t) = Length of the diffusive film
- D_{film} = Growth coefficient of the liquid film

This corresponds to the experimentally found √t-dependence in this study of the length of the spreading zone L_{SP} on time. Therefore:

$$m_{SP} = \sqrt{D_{film}} \qquad [14]$$

According to Popescu et al., D_{film} depends on the geometry of the substrate, the type of metal, the composition of the alloy and the temperature.[38]*Are micro droplets droplets consisting of condensed water?*

If a liquid film with a thickness of e_{min} spreads outwards from a macroscopic primary droplet during pseudo-partial wetting, only enough liquid should be transported to form this film. The question arises as to where the excess liquid in the spreading zone, which is assumed to be responsible for the formation of micro droplets, comes from. No reference to the formation of micro droplets on the liquid film was found in the literature on the subject of pseudo-partial wetting. A special feature of secondary spreading should be noted here: The liquid film is highly alkaline and NaOH, which is a component of the solution in the spreading zone, is highly hygroscopic. In addition, the micro droplets grow faster with increasing NaOH concentration and the literature reports an inhibition of secondary spreading when the pH value is lowered.[1,2,8,10,11] Zhang et al. also described that the size of micro droplets increases with relative humidity[6] and Bian et al. that micro droplets can disappear when the relative humidity is lowered.[5]

The dependence of the micro droplet size on the NaOH concentration and on the ambient humidity can be explained by the condensation of atmospheric moisture on the alkaline and hygroscopic liquid film. If micro droplets are droplets of condensed water on a solution film, the same laws should apply to the growth of micro droplets as to the growth of droplets during condensation due to a temperature difference.

The basic characteristics of the growth of droplets formed by condensation on a supercooled substrate are briefly described below based on the work of Medici et al. They made the following assumptions:

- The droplet shape is a spherical cap
- The transport of water molecules to the droplet surface is a purely diffusive process
- The droplet temperature is maintained constant at the temperature of the substrate
- The droplet is in humid air at given temperature and vapor pressure.

The condition of isothermal droplets should be fulfilled by a substrate with high thermal conductivity and, in the case of large droplets, also by a Marangoni flow.[39] The Marangoni flow is due to a gradient in the surface tension along the droplet interface.[40]

There are four growth stages of condensing droplets: I. nucleation, II. separate growth, III. growth with coalescence of droplets and IV. droplet nucleation between neighboring droplets. For growth in stage III. with coalescence of droplets, which was also observed for the micro droplets in the spreading zone, the mean radius of the droplets <R> increases linearly with time t:[39]

$$<R> = kt \qquad [15]$$

$$k = \frac{D(c_\infty - c_\theta)}{\varepsilon^2 f(\Theta)\zeta\rho_w} \qquad [16]$$

- <R> = Mean droplet radius
- c_∞ = Concentration of water monomers in mass per volume in the environment at the border of the concentration boundary layer ζ, corresponding to the water vapor pressure at air temperature
- c_0 = Concentration of water monomers in mass per volume at the droplet surface directly above the solution, corresponding to the water saturation pressure at the droplet temperature
- D = Water vapor diffusion coefficient in air
- ε^2 = Degree of surface coverage with droplets
- f (Θ) = Function of the contact angle Θ
- ρ_W = Density of water
- ζ = Thickness of the water vapor concentration profile

In stage III, the term ε^2 f(Θ) is approximately constant. If the diffusion coefficient is also constant, k is therefore a factor that depends only on the water vapor supersaturation $\Delta c = c_\infty - c_0$ and the thickness of the water vapor concentration profile ζ:[39]

$$k \sim \frac{(c_\infty - c_\theta)}{\zeta} \qquad [17]$$

The growth of the water droplets formed by condensation described in stage III matches the observed growth of the micro droplets in the spreading zone. The radius or diameter of the micro droplets also grows linearly with time on average.

For the described condensation due to a temperature difference between substrate and air, c_∞ refers to the temperature in the air and c_0 to the colder temperature of the droplet. For micro droplets form secondary spreading, it should be noted that the difference in the water vapor partial pressure p or the water concentration c in the environment and directly in front of the droplet surface does not come from a temperature difference, but from the reduction in vapor pressure p_0 directly above the solution due to dissolved salts.

For equal temperatures of droplet and air, instead of the vapor pressure p or the water concentration c, the relative humidity φ can be used. This connection is deduced below.

The supersaturation Δc is the difference between the water concentration directly above the droplet surface c_0 and infinitely far

away from it c_∞. The water vapor concentration c is linked to the water vapor partial pressure p via the ideal gas equation:

$$pV = nRT = \frac{m}{M}RT \quad [18]$$

- p = Pressure
- V = Volume
- n = Number of moles
- M = Molar mass
- m = Mass
- R = General gas constant
- T = Temperature

The mass concentration c is:

$$c = \frac{m}{V} = p\frac{M}{RT} \quad [19]$$

The relative humidity φ is the quotient of water vapor partial pressure p and water saturation pressure p_S.[41]

$$\varphi = \frac{p}{p_{s.}} \quad [20]$$

This means that c is directly proportional to φ:

$$c = \varphi\frac{p_s M}{RT} \quad [21]$$

Therefore, at constant temperature, the droplet growth constant k or m_M is dependent on the difference between the relative humidity directly above the droplet surface φ_0 and the relative humidity in the environment φ_∞, as well as the thickness of the humidity profile ζ:

$$k \sim \frac{(\varphi_\infty - \varphi_0)}{\zeta} \quad [22]$$

The dependence of the factor k on the water vapor supersaturation Δc could explain the dependence of the micro droplet growth rate m_M on the NaOH concentration and the air humidity.

From Eq. 22 it follows:

- If $\varphi_\infty > \varphi_0$, k is positive, micro droplets can grow
- If $\varphi_\infty < \varphi_0$, k is negative, no micro droplets grow and existing micro droplets evaporate
- The greater the amount of the difference $(\varphi_\infty - \varphi_0)$, the faster micro droplets grow or shrink

Soluble salts can lower the humidity above an aqueous solution φ_0 by reducing the vapor pressure p.[22] If micro droplets are water droplets formed by condensation, this explains the increasing growth rate m_M of micro droplets with NaOH concentration, since $(\varphi_\infty - \varphi_0)$ would increase with increasing NaOH concentration. It also explains the observations of Zhang et al. that the number and size of micro droplets increase with the relative humidity of the environment φ_∞[6] and Bian et al. that micro droplets on steel can disappear when the relative humidity in the environment φ_∞ decreases.[5]

Interpretation of the E_{corr} profile with secondary spreading.— The measured E_{corr} profile of a NaCl droplet on steel with secondary spreading is to be interpreted using estimated current-voltage curves based on the known mechanism of droplet corrosion according to Evans.[42,43] The assumed qualitative current-voltage curves are shown in Fig. 15. According to Evans, a large corroding droplet can be regarded as an aeration element, whereby the oxygen concentration in the solution is higher at the edge of the droplet than in the center of the droplet due to the lower electrolyte layer thickness. This is why the cathode forms at the edge of the droplet and the anode in the center of the droplet.[42]

The anodic region with strong iron dissolution in the center of the droplet and the cathodic region with passive steel substrate at the edge of the droplet were found to be consistent. In the anodic region in the center of the droplet, the anodic partial current curve of the iron

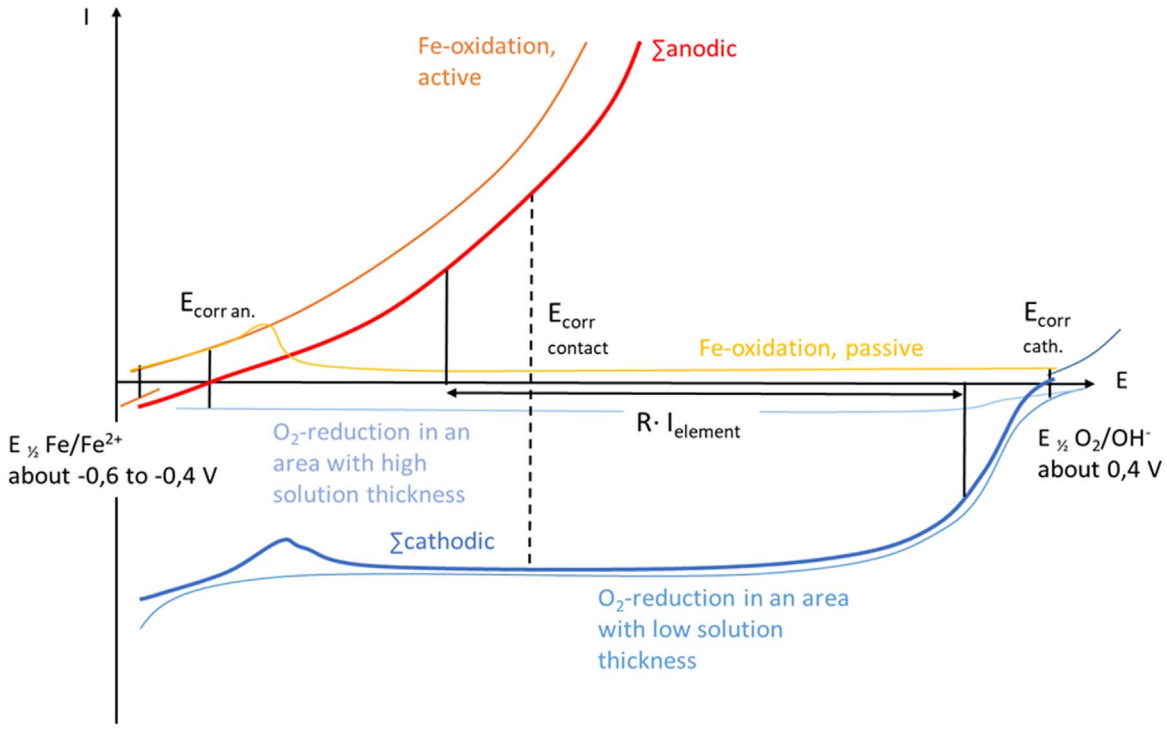

Figure 15. Assumed qualitative current-voltage curves for an area in the center of the droplet (anodic area) and for the edge of the droplet (cathodic area).

dissolution should be steep due to the neutral to slightly acidic pH value. The cathodic partial current curve, on the other hand, is in the limiting current range and very low, as the oxygen concentration is low due to the thick electrolyte layer. The total current curve in the anodic range shows that under these conditions E_{corr} is very low and should be slightly above the half-cell potential of the iron dissolution.

In the cathodic area at the edge of the droplet, the oxygen concentration is high due to the very low electrolyte layer thickness and the cathodic limiting current density of the oxygen reduction is considerably greater than in the anodic area. However, due to the high pH value at the edge of the droplet, the steel is passive. Due to the low passive residual current density, E_{corr} is very high, slightly below the halfcell potential of the oxygen reduction. This should also apply to the spreading zone from secondary spreading.

Cathodic and anodic areas within the droplet are conductively connected by the steel substrate and the electrolyte. Assuming that this circuit has no electrical resistance R between anodic and cathodic zone, this would result in a uniform $E_{corr\ contact}$ for the entire droplet, which lies between the hypothetical non-contact E_{corr} in the anodic and cathodic areas with an imaginary complete separation of the two areas. If a resistance between the anodic and the cathodic area greater than 0 is assumed, the element current decreases and $E_{corr\ contact}$ decreases in the anodic region, while $E_{corr\ contact}$ increases in the cathodic region. The higher the resistance in the system, the closer $E_{corr\ contact}$ approaches the hypothetical non-contact E_{corr} in the anodic or cathodic range. Only $E_{corr\ contact}$ can be measured. It is therefore important to estimate the resistance between the anodic and cathodic areas. The electrolyte resistance is assumed to be the greatest resistance in the system.

In the following, the resistances between different points in the cathodic zone (including the spreading zone) and the anodic zone will be estimated. Within the cathodic zone it is assumed that the resistance between a point in the cathodic zone and the anodic/cathodic zone boundary is crucial, as it should be smaller than the resistance between the same point in the cathodic zone and a more distant point in the anodic zone. The resistances discussed below therefore always refer to a specific point in the cathodic zone or the spreading zone in relation to the anodic/cathodic zone boundary.

Using this assumption and the current-voltage curves assumed in Fig. 15, the potential profile shown in Fig. 13 of a large NaCl droplet of 100 µl measured with SKP and can be explained.

In Fig. 16, the right half of this droplet is shown schematically and divided into four areas: anodic area, cathodic area, spreading zone and periphery.

In the anodic and cathodic areas, which are both located within the droplet, a low electrolyte resistance is to be expected due to the saline solution. Therefore, the resistance in the cathodic zone should only increase slightly with the distance to the anocid/cathodic zone boundary. This should results in a slight difference between $E_{corr\ contact}$ the anodic and cathodic area. In fact, the potential profile in Fig. 13 shows a slight step between the anodic and the cathodic area. It was observed during the SKP measurement that the position of this step actually coincides with the boundary of the anodic and cathodic regions. At −300 to −250 mV vs SHE, the potential in the anodic range is above the expected halfcell potential of −600 to −400 mV vs SHE of the iron dissolution in the slightly acidic range (see Fig. 15) and thus matches the expected $E_{corr\ contact}$ with low electrolyte resistance.

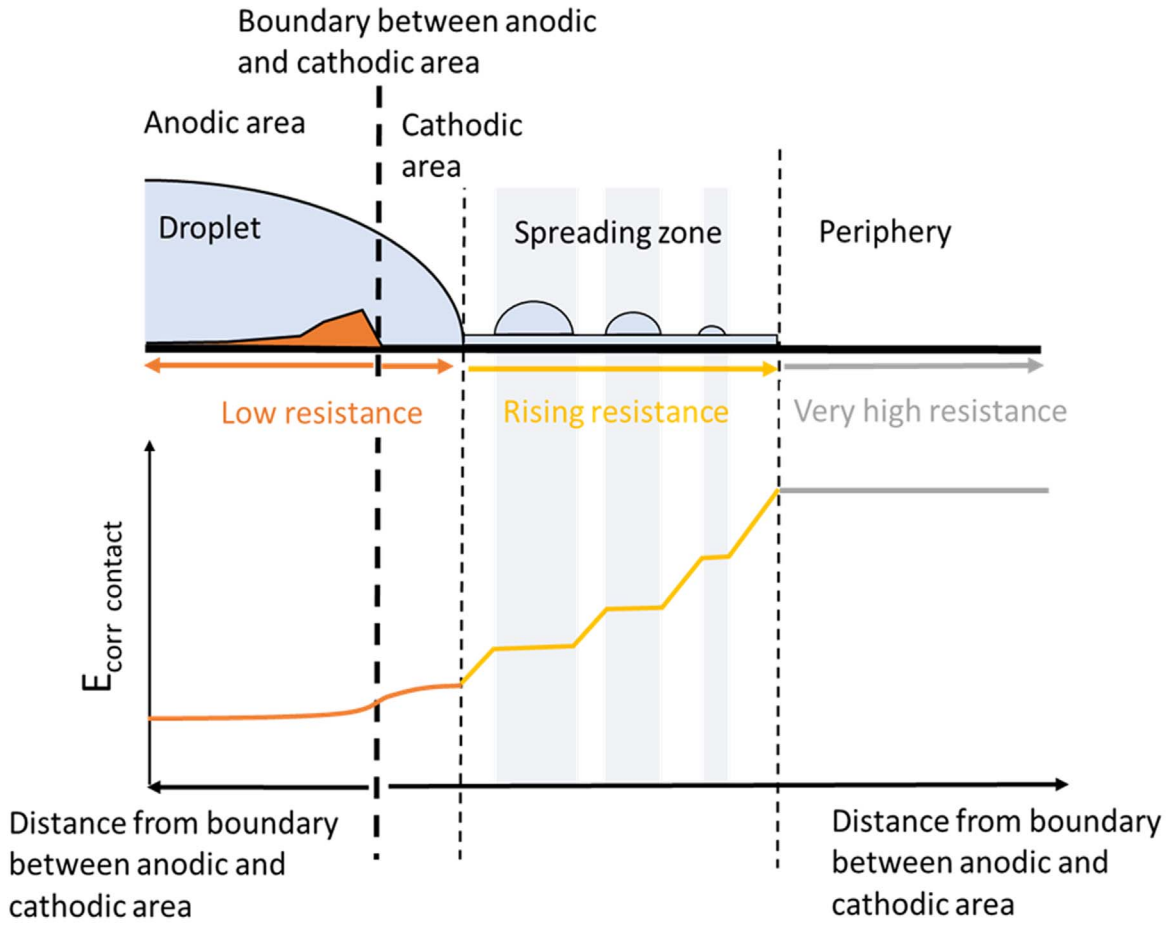

Figure 16. Explanation of the $E_{corr\ contact}$ potential profile of a 100 µl NaCl droplet on steel measured with SKP by estimating the electrolyte resistance between different areas and the anodic/cathodic boundary. The hypothetical current-voltage curves shown in Fig. 14 are used as a basis.

A potential increasing from the edge of the droplet to the periphery was measured within the spreading zone. Large micro droplets within the spreading zone lower the potential and flat "potential shoulders" are formed. As described, the spreading zone can be regarded as a very thin electrolyte film with water droplets formed by condensation. It is therefore reasonable to assume a high resistance between points in this area and the anodic/cathodic zone boundary, which increases with the distance to the edge of the droplet. In general, the resistance should increase with the distance to the boundary between the anodic and cathodic areas. However, this effect is barely visible within the cathodic zone due to the low electrolyte resistance, whereas it is clearly visible in the spreading zone with high electrolyte resistance. This effect also explains the potential shoulders at micro droplets. Within micro droplets, the electrolyte layer thickness is considerably higher and the electrolyte resistance considerably lower than in the spreading film, which is why the resistance increases only slightly with the distance to the boundary and the potential profile is almost horizontal within micro droplets.

The higher the resistance between a point within the spreading zone and the anodic/cathodic zone boundary, the lower the flowing partial cathodic element current. With a lower cathodic element current, less OH^--ions would be formed in that area und the ion concentration would be less than in other areas within the spreading zone with a lower resistance between themselves and the anodic/cathodic zone boundary. If micro droplets grow faster at locations with a high ion concentration (lower humidity above the solution), the electrolyte resistance between one area in the spreading zone and the anodic/cathodic boundary could correlate with the occurrence of micro droplets.

If secondary spreading is a form of pseudo-partial wetting, the thickness of the liquid film depends on the course of the free energy function P(e) and thus on the Hamaker constant difference A and the spreading coefficient S. Since the steel used is a multiphase solid, local differences in both variables are to be expected. This could lead to locally different stable film thicknesses of the solution layer in the spreading zone. This means that there could be paths between points in the spreading zone and the anodic zone that lead through thicker areas of the film and have a lower electrolyte resistance. In these areas, the cathodic partial element current would be higher, the potential lower and more OH^- would be formed due to the accelerated oxygen reduction. The migration of Na^+ for charge equalization would also be facilitated. A higher ion concentration would occur in these areas, which would lead to a lower humidity above the solution surface and cause the formation of a micro droplet. If this were the case, the resulting micro droplets would directly indicate areas with increased cathodic activity.

Conclusions

A probable mechanism of secondary spreading can be deduced from the discussed experimental results and theoretical models:

Secondary spreading is triggered by a strongly alkaline pH value. This changes the shape of the free energy function P(e) from partial to pseudo-partial wetting, either by changing the Hamaker constant difference A, the spreading coefficient S or both. In the case of pseudo-partial wetting, a diffusive alkaline liquid film with a defined thickness e spreads outwards and forms the spreading zone.

The rate of spreading is determined on the one hand by the diffusion rate of the cation in the initial droplet and on the other hand by the substrate. The influence of the substrate could possibly be explained by a change in the Hamaker constant difference A or the spreading coefficient S, both of which can change the shape of the energy function P(e) and thus shift the position of the energetic minimum. This changes the stable film thickness e_{min}. A thicker film could accelerate the diffusion of the cations and a thinner film could decelerate it.

Micro droplets are formed by water condensation from the air on the alkaline hygroscopic spreading film. Due to the defined film thickness, excess water does not lead to a thicker film, but to accumulation in droplets.

Due to the potential profile and the resulting high resistance within the spreading zone, the proportion of secondary spreading in the cathodic partial current is estimated to be low compared to the cathodic zone at the edge of the droplet.

ORCID

Lea Seeger https://orcid.org/0000-0001-8521-3993
Wolfram Fürbeth https://orcid.org/0000-0003-3850-0943

References

1. A. K. Neufeld, I. S. Cole, A. M. Bond, and S. A. Furman, "The initiation mechanism of corrosion of zinc by sodium chloride particle deposition." *Corros. Sci.*, **44**, 555 (2002).
2. M. Liu, Q. Yin, Y. Liu, C. Pan, C. Wang, and Z. Wang, "Secondary spreading of acidified aerosols on the surface of Zn." *Journal of Materials Research and Technology*, **9**, 2635 (2020).
3. T. Tsuru, K. Tamiya, and A. Nishikata, "Formation and growth of micro-droplets during the initial stage of atmospheric corrosion." *Electrochim. Acta*, **49**, 2709 (2004).
4. I. S. Cole, T. H. Muster, S. A. Furman, N. Wright, and A. Bradbury, "Products Formed during the Interaction of Seawater Droplets with Zinc Surfaces from 1- and 2.5-Day Exposures." *J. Electrochem. Soc.*, **155**, C244 (2008).
5. L. Bian, Y. Weng, and X. Li, "Observation of micro-droplets on metal surface in early atmospheric corrosion." *Electrochem. Commun.*, **7**, 1033 (2005).
6. J. Zhang, J. Wang, and Y. Wang, "Electrochemical investigations of micro-droplet formed on metals during the delisquescence of salt particles in atmosphere." *Electrochem. Commun.*, **7**, 443 (2005).
7. J. Wang, L. Liang, and J. Jiang, "The role of electrochemical polarization in micro-droplets formation." *Electrochem. Commun.*, **10**, 1788 (2008).
8. Z. Y. Chen, D. Persson, and C. Leygraf, "Initial NaCl-particle induced atmospheric corrosion of zink - Effect of CO_2 and SO_2." *Corros. Sci.*, **50**, 111 (2008).
9. E. J. Schindelholz, H. Cong, C. F. Jove-Colon, S. Li, J. A. Ohlhausen, and H. K. Moffat, "Electrochemical aspects of copper atmospheric corrosion in the presence of sodium chloride." *Electrochimica Acta*, **276**, 194 (2018).
10. N. S. Azmat, K. D. Ralston, B. C. Muddle, and I. S. Cole, "Corrosion of Zn under acidified marine droplets." *Corros. Sci.*, **53**, 1604 (2011).
11. Z. Y. Chen, D. Persson, A. Nazarov, S. Zakipour, D. Thierry, and C. Leygraf, "In situ studies of the effect of CO_2 on the initial NaCl-induced atmospheric corrosion of copper." *J. Electrochem. Soc.*, **152**, B342 (2005).
12. A. K. Neufeld, I. S. Cole, A. M. Bond, H. S. Isaacs, and S. A. Furman, "Characterization of salt particle-induced corrosion processes by synchrotron-generated X-ray fluorescence and complementary surface analysis tools." *State-of-the-art application of surface and interface analysis methods to environmental material intractions* (The Electrochemical Society, Inc.) (2001), Electrochemical Society Proceedings –520011-56677-311-3.
13. B. E. Risteen, E. Schindelholz, and R. G. Kelly, "Marine aerosol drop size effects on the corrosion behavior of low carbon steel and high purity Iron." *Journal of The Elektrochemical Society*, **161**, C580 (2014).
14. T. H. Muster, A. Bradbury, A. Trinchi, I. S. Cole, T. Markley, D. Lau, S. Dligatch, A. Bendavid, and P. Martin, "The atmospheric corrosion of zinc: the effect of salt concentration, droplet size and droplet shape." *Electrochim. Acta*, **56**, 1866 (2011).
15. DIN Deutsches Institut für Normung e, *V. DIN EN 10130. 10772* (Beuth Verlag GmbH, Berlin) (2016).
16. H. Stern, D. R. Sadoway, and J. W. Tester, "Copper sulfate reference electrode." *J. Electroanal. Chem.*, **659**, 143 (2011).
17. M. Rohwerder and F. Turcu, "High-resolution Kelvin probe microscopy in corrosion science: Scanning Kelvin probe force microscopy (SKPFM) vs classical scanning Kelvin probe (SKP)." *Electrochim. Acta*, **53**, 290 (2007).
18. M. Rohwerder, "Passivity of Metals and the Kelvin Probe Technique." *Reference Module in Chemistry, Molecular Sciences and Chemical Engineering, Encyclopedia of Interfacial Chemistry, Surface Science and Electrochemistry*, **1**, 414–422 (2018).
19. S. Trasatti, "The absolute electrode potential: an explanatory note." *Pure & Appl Chem*, **58**, 955 (1986).
20. L. Seeger, R. Lobnig, and M. Wicinski, "New calibration method for kelvin probe in changing humidity conditions." *J. Electrochem. Soc.*, **169**, 101501 (2022).
21. N. L. Garcia de Rodriguez, W. Thielemans, and A. Dufresne, "Sisal cellulose whiskers reinforced polyvinyl acetate nanocomposites." *Cellulose*, **13**, 261 (2006).
22. E. Riedel, *Anorganische Chemie, 2., verbesserte Auflage* (Walter de Gruyter, Berlin, New York) 2nd ed. (1990)3110123215.
23. K. Schiebold, *Zerstörende Werkstoffprüfung, Metallographische Werkstoffprüfung und Dokumentation der Prüfergebnisse* (Springer-Verlag GmbH Deutschland, Berlin) (2018)978-3-662-57803-2.
24. R. Opila, C. Weschler, and R. Schubert, "Acidic vapours above satturated salt solutions commonly used for control of humidity." *IEEE Trans. Compon. Hybrids Manuf. Technol.*, **12** (1989), März F 1, 113.
25. D. R. Linde, *CRC Handbook of Chemistry and Physics* (CRC Press, Boca Raton, FL) Internet Version ed. (2005).

26. H. H. King, L. Hall, and G. C. Ware, "A study of the density, surface tension and adsorption in the water-ammonia system at 20°." *Journal of the American Chemical Society*, **52**, 5128 (1930).
27. T. Yuan, J. Wang, and Z. Li, "Measurement and modelling of solubility for calcium sulfate dihydrate and calcium hydroxide in NaOH/KOH solutions." *Fluid Phase Equilib.*, **297**, 129 (2010).
28. G. Whipple and A. Mayer, "The solubility of calcium carbonate and of magnesium hydroxide and the prcipitation of these salts with lime water." *Public Health Papers and Reports*, **31**, 151–165 (1905).
29. K. Popov, L. Lajunen, A. Popov, H. Rönkkömäki, M. Hannu-Kuure, and A. Vendilo, "7Li, 23 Na, 39 K and 133 CsNMR comparative equilibrium study of alkali metal cation hydroxide complexes in aqueous solutions. First numerical value for CsOH formation." *Inorg. Chem. Commun.*, **5**, 223–225 (2002).
30. A. Leng, H. Streckel, and M. Stratmann, "The delamination of polymeric coatings from steel: Part 2. First stage delamination, effect of type and concentration of cations on delamination, chemical analysis of the interface." *Corros. Sci.*, **41**, 579 (1999).
31. N. Khayatan and M. Rohwerder, "A new insight into the rate determining step of cathodic delamination." *Corros. Sci.*, **202**, 1 (2022).
32. H. Seiler, "Secondary electron emission in the scanning electron microscope." *J. Appl. Phys.*, **54**, 1 (1983).
33. R. E. Lobnig, R. P. Frankenthal, J. D. Sinclair, and M. Stratmann, "Mechanism of atmospheric corrosion of copper in the presence of submicron ammonium sulfate." *J. Electrochem. Soc.*, **141**, 2935 (1994).
34. L. Leger and J. Joanny, "Liquid spreading." *Rep. Prog. Phys.*, **55**, 431–486 (1992).
35. F. Brochard-Wyart, "Spreading of nonvolatile liquids in a continuum picture." *Langmuir*, **7**, 335 (1991).
36. E. Petek and R. Katsumata, "Open questions that can bridge intermolecular interactions and macroscopic wetting/dewetting behaviors of thin films." *Macromol. Chem. Phys.*, **224**, 2200375 (2023).
37. C. Xie, "Properties and experimental studies of precursor film in dynamic wetting." *6th International Conference on Mechanical Engineering and Automation Science (ICMEAS)*195 (2020).
38. M. N. Popescu, G. Oshanin, S. Dietrich, and A. Cazabat, "Precursor films in wetting phenomena." *J. Phys. Condens. Matter*, **24**, 1 (2012).
39. M. Medici, A. Mongruel, L. Royon, and D. Beysens, "Edge effects on water droplet condensation." *Physical Review E*, **90**, 062403 (2015).
40. R. Seemann, J. Fleury, and C. C. Maass, "Self-propelled droplets." *The European Physical Journal, Special Topics*, **225**, 2227 (2016).
41. M. Dehli, E. Doering, and H. Schedwill, *Grundlagen der Technischen Thermodynamik* (Springer Fachmedien Wiesbaden GmbH, Wiesbaden) 9 (2020), Auflage 978-3-658-31727-0.
42. H. Kaesche, *Die Korrosion der Metalle, Physikalisch-chemische Prinzipien und aktuelle Probleme* (Springer-Verlag Berlin, Heidelberg, New York) (1966) 3540088814.
43. U. R. Evans, "Some recent work on the corrosion of metals." *Metal Ind*, **29**, 481 (1926).